RSC Advances

REVIEW

View Article Online
View Journal | View Issue

A review on advances in photocatalysts towards CO_2 conversion

Cite this: *RSC Adv.*, 2014, **4**, 20856

Sreejon Das[ab] and W. M. A. Wan Daud*[a]

The present situation reveals the dependence on fossil fuels, which is seriously accountable for two major impediments: (i) global warming due to increasing atmospheric carbon dioxide (CO_2) and (ii) the alarming consumption of energy assets. The reduction of green CO_2 in terms of producing solar fuels would be an expedient accomplishment to resolve both problems, simultaneously. The review classifies different categories of photocatalysts applied in foregoing photocatalytic CO_2 conversion processes with detailed information concerning operating conditions, preparation techniques and physical properties of catalysts, radiation sources, and selectivity. The categories are concentrated on metal oxides, sulfides, phosphides, and p-type and nonmetal oxide semiconductors. In addition, their modification by doping co-metals, noble metals, transition metals and non-metals for visible light response is emphasized. Besides, for harnessing solar fuel, the recent prospect and advancement of novel sensitized catalysts by dye elements, phthalocyanines and quantum dots (QDs) are also highlighted in this review. This technology needs more efficient solar active catalysts to increase production rates as well as selectivity. The recent scenario indicates that massive prospects and opportunities still exist in this area for further investigation on catalyst selection.

Received 28th February 2014
Accepted 8th April 2014

DOI: 10.1039/c4ra01769b

www.rsc.org/advances

1. Introduction

World energy consumption has deep implications for humanity's social-economic-political sphere. For this reason, the global energy map is changing with potentially extensive consequences for energy markets and trade, and also by a

[a]*Department of Chemical Engineering, Faculty of Engineering, University of Malaya, 50603 Kuala Lumpur, Malaysia. E-mail: ashri@um.edu.my*

[b]*Department of Chemical Engineering & Polymer Science, Shahjalal University of Science & Technology, 3114 Sylhet, Bangladesh*

Sreejon Das is a postgraduate research student in the Department of Chemical Engineering at University of Malaya, Malaysia. He graduated with Distinctions in 2009, from the Department of Chemical Engineering and Polymer Science, Shahjalal University of Science and Technology (SUST), Sylhet, Bangladesh. He then began his career as a team member (Environment, Safety, Health and Chemical Management) in the Youngone Group of Industries Ltd., Chittagong, Bangladesh. Beginning on 19 September 2010, he joined as a full-time 'Faculty Member' in the department of Chemical Engineering and Polymer Science, SUST, Sylhet, Bangladesh, where he continues today. He is now conducting his research work in "Photocatalytic Conversion of CO_2 into Hydrocarbon Fuels" at the University of Malaya.

Professor Wan Mohd Ashri Bin Wan Daud earned his bachelor's degree in chemical engineering in 1991 at Leeds University, Leeds, UK and his master's degree in chemical engineering in 1992 from the University of Sheffield, Sheffield, UK. He earned his PhD degree in Chemical Engineering in 1996 at the University of Sheffield. Since 2005, he has worked as Professor of Chemical Engineering at the University of Malaya. His research fields include energy, biomass conversion and the synthesis of catalyst materials, catalysis, zeolites, polymerization process, separation process (adsorption, activated carbon, and carbon molecular sieve); ordered mesoporous materials, and hydrogen storage materials. Professor Wan Mohd Ashri Bin Wan Daud has written approximately 90 research papers that have been published.

growing world population.[1–3] On the other hand, the world is gradually becoming aware that essential alterations will be required to meet the growing demand for energy. Maximum energy sources are inadequate to satisfy the growing global energy demand, which will double by 2050 and triple at the end of this century.[4] According to the U.S. Energy Information Administration,[5] energy consumption rates remained vigorous in several developing countries, specifically in Asia (>4%). In North America, Europe and the Commonwealth of Independent States, consumption fell by 4.5%, 5% and 8.5%, respectively, because of economic breakdown.

Energy produced from fossil fuels has great importance because the latter can be burned (oxidized to carbon dioxide and water), producing significant amounts of energy per unit weight.[6] Non-renewable fossil fuels yield takes millions of years, and these assets are being exhausted much faster than new ones are being made. Fossil fuel consumption is also threatening to the environment. During the period from 1961 to 2010, the British Petroleum Statistical Review of World Energy 2013[7] estimated that the rate of energy consumption has shown an upward trend. Worldwide movement towards renewable energy production is therefore in progress to meet increased energy requirements. The main renewable sources such as sunlight, wind, tides, waves, geothermal heat, biomass and nuclear energy offer electricity with zero carbon dioxide emissions.[8] Energy conversion from waste is one of the supportable sources to convert the unwanted biomass into 7 to 10 TW of energy.[9–11] Other renewable sources like wind, hydroelectric and tide/ocean currents provide almost 2.1 TW, 1.5 TW and <2 TW of energy respectively.[12] Conversely, these renewable sources are quite limited to meet the overall energy demand.

To fulfil the energy demand, nuclear energy, which generally is the part of the energy of an atomic nucleus released by fusion or fission or radioactive decay could be a promising renewable source. Currently, approximately 14% of the world's electric energy is provided by the nuclear energy.[13] On the other hand, the protection of nuclear reactors is a forthcoming limitation of nuclear chain-reaction control, and safe storage of the extremely radioactive nuclear waste is still an unidentified pathway towards a low fossil-fuel consumption future.[14] Natural disasters like earthquakes may have harmful impacts on the earth from the nuclear plants. Moreover, nuclear power is not able to produce liquid fuel for transportation purposes. Unlike nuclear energy, another sustainable and abundant source of energy is required without the introduction of harmful environmental effects.

Renewable solar energy is used to harness the sun's energy and convert it into usable products through solar heating,[15,16] solar photovoltaics,[17,18] solar thermal electricity,[19] solar architecture,[20,21] and artificial photosynthesis.[22] The satisfaction of global energy needs for an entire year is achievable by harnessing solar energy on the Earth's surface. Solar fuel is formed by utilizing light to produce chemical energy[23,24] by artificial photosynthesis, or thermochemical reaction. The development of inexpensive, limitless and clean solar energy technologies must have massive and long-term benefits. This progress will intensify global energy reserves through dependence on an original, infinite and mostly import-independent resource, increase sustainability, decrease pollution, lower the costs of mitigating climate change, and keep fossil-fuel prices lower than through other means.

Besides energy needs, sufficient physical evidence suggests that climate change is mainly responsible for carbon dioxide emissions from fossil-fuel burning.[25–27] As stated by the International Energy Agency (2012),[28] the goal of decreasing climate warming by 2 °C is becoming more difficult and costly each passing year. All tolerable carbon dioxide emissions would be locked-in by the remaining energy infrastructure if appropriate steps are not taken before 2017. Already, global carbon dioxide growth in the atmosphere was amplified by around 1.5 ppm (8 billion tons) per year from 1975 to 2002. Basically, the atmospheric carbon dioxide level inflated much more quickly by 2.25 ppm (12 billion tons) per year. Every year, more than 10 billion tons of carbon dioxide is added to our atmosphere.[29] As estimated by the U.S. Department of Energy,[30] natural processes can only absorb about half that amount.

Abundant CO_2 can be an asset by using appropriate applications in solar-fuel transformation. The recycling process of CO_2 can regulate global warming as well as fuel demand.[31] Besides photocatalytic conversion of CO_2, other conversion processes can turn CO_2 into fuels illustrated in Fig. 1, but the disadvantages in those processes are the high temperature and high electrical voltage requirements to break down the CO_2 molecules, limitations of raw materials, high-cost operation, and unsustainability. Photocatalytic transformation of CO_2 into solar fuel is more sustainable and favorable than other technologies because of zero addition of additional energy consumption and environmental deterioration. In the beginning, photocatalytic CO_2 conversion was conducted by an artificial lamp. Recently, interest has grown in the harnessing of solar power by advanced photocatalytic processes. The stability of catalysts and mild operating conditions are among the most significant reasons for choosing this technology.[32,33] However, more intensive study and improvement are required to select active solar-driven novel catalysts and effective architecture of solar photoreactors for industrial applications. Moreover, there are some unanswered questions in this technology with the selectivity of the photocatalytic reactions and limited efficiency.

This paper concentrated on advancements in the photochemical transformation of CO_2 into hydrocarbon fuels. The second chapter of this paper provides a snapshot of current developments in the photocatalytic reduction of CO_2 on various types of semiconductors. Pure metal oxide semiconductors are cheap and the most commonly used photocatalysts in this technology like TiO_2. To a large extent, this can be ascribed to its band structure, which is acceptable, but certainly not optimal for the reduction of CO_2 driven by solar energy. The wide band gap (3.2 eV) limits the absorption of light into the UV range. The modification of metal oxide semiconductors by supporting materials helps to control the catalysts' size from crystal growth and facilitate the response towards visible light. The two most common methods for extending the absorption range to visible light are sensitization and doping. Doping metal on semiconductors acts as an electron trap to provide the electrons to

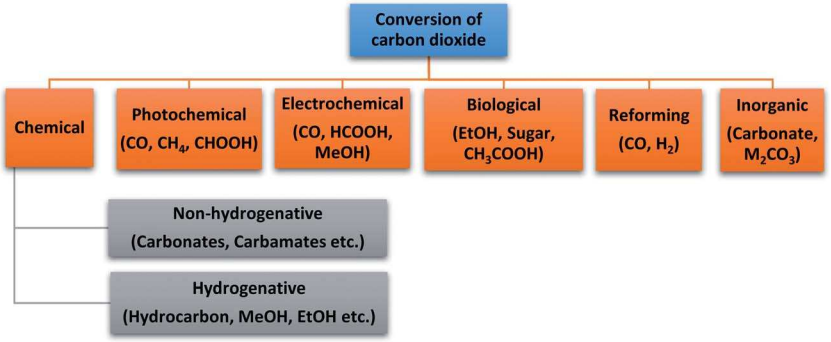

Fig. 1 Well-known CO_2 transformation paths with potential products.[34]

the CO_2. Besides, non-oxide semiconductors initially received a lot of attention. For example, the valence band of sulphide semiconductors is made of 3p orbitals of the sulfur atoms and is shifted upwards, compared with those of the oxide analogues, while the conduction band electrons are also more reductive.[35] Interest has grown in the involvement of flexible substrates because they deliver a high surface area for catalysts on the films of substrates. In the mainstream, the review categorizes the different types of photocatalysts used in previous photocatalytic conversions of CO_2 processes (with detailed information regarding the operating conditions, preparation techniques and physical properties of catalysts, radiation sources and selectivity) based on metal oxides, sulfides, phosphides, and p-type and non-metal-oxide semiconductors. In addition, these processes highlighted their modifications by doping co-metals, noble metals, transition metals and non-metals for visible light responses. Besides, the recent prospect and advancement of novel sensitized catalysts by dye elements, phthalocyanines and quantum dots (QDs) for harnessing solar fuels are prominent in this review.

2. Photocatalytic CO_2 transformation based on catalysts

The transformation of CO_2 into fuel by using solar light irradiation is an effective method because there is no addition of extra energy and no negative influence on the environment. The immediate requirement in this technology is to develop visible light-sensitive photocatalysts, which are prominent in CO_2 recycling. Different types of photocatalysts have been already introduced by many researchers in this technology. Some of the catalysts exhibited high conversion rates and selectivity under visible light irradiation, while other catalysts were not feasible for visible light response and presented low yield rates. Researchers are still trying hard to advance the properties of catalysts in terms of solar fuel production. The reaction mechanism of selective photocatalysts under light irradiation is illustrated in Scheme 1. A concise classification of photocatalysts is also shown in Fig. 2, based on the recent development in photocatalytic CO_2 transformation.

2.1 Metal oxide photocatalysts

Metal oxides as light-sensitive catalysts have been applied in several processes such as the breaking down of organic and inorganic materials to valuable products,[23,36,37] water treatment,[38,39] and self-cleaning[40,41] processes. The leading approach of using metal oxide catalysts in CO_2 conversion to carbonaceous fuel was introduced by Inoue *et al.*[42] Variations in metal oxide photocatalysts have already been introduced by integrating foreign elements and other compounds with different supportive substrates[43–46] for lessening its particle size, controlling its crystal growth, and increasing its surface area and pore volume. Various metal oxide photocatalysts, which were frequently studied in many photocatalytic CO_2 reduction processes, are characterized in this section with sufficient information.

2.1.1 Surface unmodified metal oxide photocatalysts. TiO_2 is a frequently used metal oxide in the photocatalytic transformation of CO_2 into hydrocarbon fuel because it is an inert, corrosion-resistant and inexpensive semiconductor. In nature, TiO_2 is established as three familiar minerals such as rutile, anatase and brookite. Among them, rutile and anatase phases indicate better efficiency under light radiation. Mutually, anatase and rutile phases reveal definite band gap energy at around 3.2 eV and 3.0 eV, respectively. The rutile phase is capable of absorbing visible light because of its comparatively low band gap energy, while the anatase form only displays its response to ultra-violet (UV) irradiation. Thus, the rutile phase is not used due to its ineffective photoactivity; the best photoactivity can be achieved by combining anatase with a slight amount of rutile.[47] A clear idea of metal oxide semiconductors used in various studies for photocatalytic CO_2 transformation is represented in Table 1. The light absorption by titanium-dioxide semiconductor is effective, while the semiconductor exhibits high surface area. The surface area of TiO_2 is indirectly proportional to the size of particle; conversely, the size of the particle is directly proportional to the band gap energy. The semiconductor shows high band gap energy as a result of the shifting of valence band energy to lower energies after a certain decrease in the particle size, whereas band energy is intensely shifted to higher energies.[48] On the other hand, significantly narrow band gap energy leads to inadequate redox potential to achieve oxidizing and reducing reactions. Therefore, it is

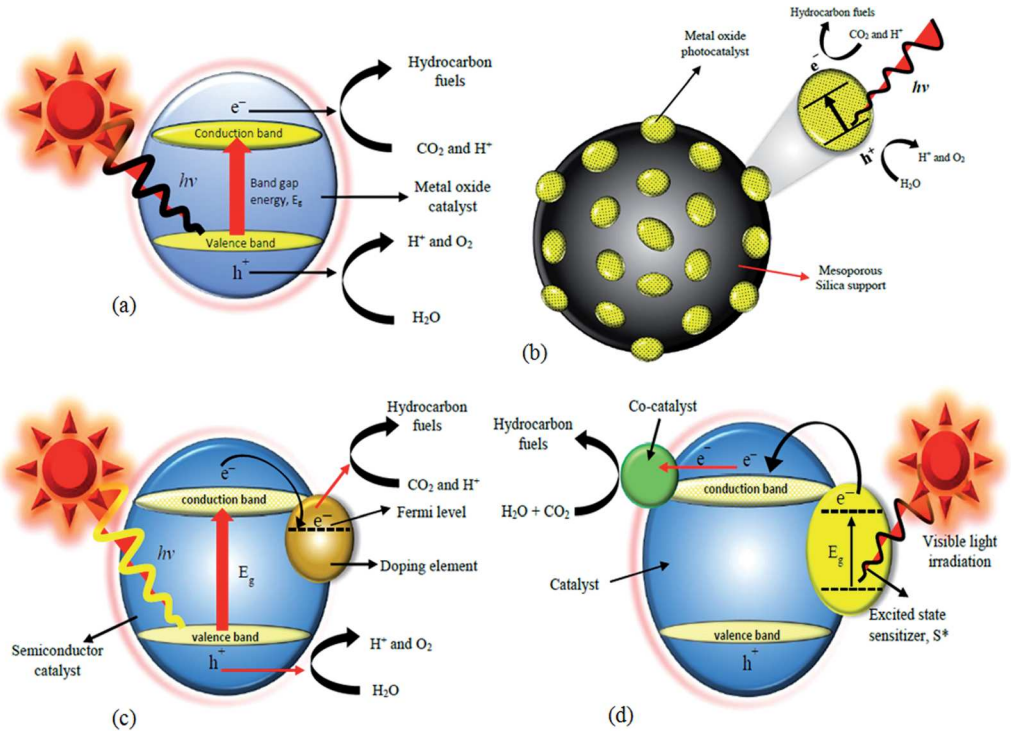

Scheme 1 Photocatalytic reaction mechanism of (a) an unmodified metal oxide semiconductor; (b) supported metal oxide semiconductor; (c) doped semiconductor; and (d) dye sensitized semiconductor under light irradiation.

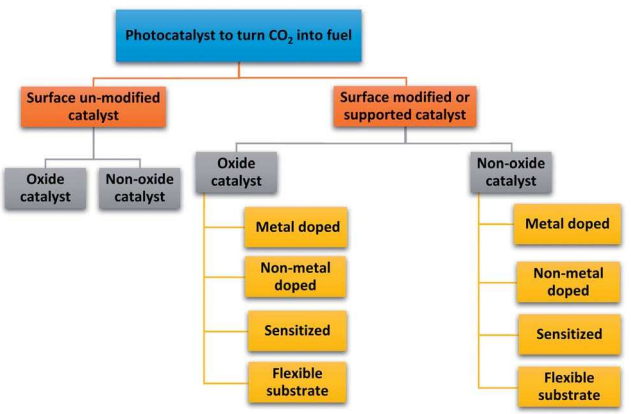

Fig. 2 Classification of photocatalysts on CO_2 transformation into fuel.

compulsory to fix a structure that exhibits a settlement between the particle size and band gap energy range.[49] Tan *et al.* investigated a combination of 80% anatase and 20% rutile forms as a photoactive catalyst.[50] In Scheme 1(a), the photocatalytic conversion mechanism of CO_2 on unmodified metal oxide semiconductor is sketched.

Commercial Degussa P25 is found to be slightly less active than modified TiO_2 (anatase and rutile).[51] It is indicated that unmodified TiO_2 (P25) metal oxide semiconductors generally have high surface area as well as an affinity to organic impurities on their surfaces to facilitate the adsorption of organic compounds, which have the potential to perform as both an electron donor and a carbon source for the products.[52] Besides, this type of metal oxide catalyst expresses better methane production, compared with the Degussa P25 treated by calcination and washing where CO is the major product.[52,53] In various studies, product dissimilarity is also observed due to the treatment procedure on anatase TiO_2 in several methods.[54–56] For instance, treatment by the acidic solutions (1 M nitric acid) is suitable for formic acid formation due to the protonation of reaction intermediates into the reaction medium.[54] Treatment with 2-propanol acts as a hole scavenger in CO_2 photoreduction with anatase TiO_2, where the methane formation rate was considerably higher. In addition, it was observed that in absence of 2-propanol, no methane was found.[56] Moreover, the synthesis of TiO_2 by the sol–gel method removes the presence of small brookite nanoparticles that normally arise in low-temperature formation reactions and considerably hinder the phase alteration to rutile at elevated temperatures.[48,57]

Some prospective metal oxide photocatalysts other than TiO_2 were reported in many investigations. Inoue *et al.* studied three metal oxides, TiO_2, ZnO and WO_3, to understand their photocatalytic characteristics under UV light radiation.[42] It was found that the yield of methyl alcohol increased as the conduction band becomes more negative with respect to the redox potential of H_2CO_3/CH_3OH, whereas methyl alcohol was not produced in presence of the WO_3 catalyst, which has a conduction band more positive than the redox potential of H_2CO_3/CH_3OH. However, WO_3 possesses low band gap energy (2.8 eV) with respect to visible light irradiation. G. Xi *et al.* synthesized the $W_{18}O_{49}$ catalyst in the form of nanowires with band gap energy

Table 1 Advances in surface unmodified metal oxide catalysts for CO_2 photoreduction[a]

Researcher (year) and ref.	Catalyst/band gap energy	Catalyst treatment technique	Reactants (amount)/radiation source/light intensity	Operating variables (T/P/pH/t/QE), physical properties (W/SA/PS/SC/MP)	Major product/yield (μmol h^{-1} per g catalyst)/efficiency (%)	Comments
G. Xi *et al.* (2012)[58]	$W_{18}O_{49}$/2.7 eV	One-pot solution-phase method	CO_2 (saturated), water vapor (—)/visible light (>420 nm)/—	(343/—/—/6/—), (—/—/nanowires with 1 nm/—/supported)	Methane/666[b]/—	• Ultrathin nanowires indicate strong light absorption from the visible light to the NIR regions • All oxygen vacancies in the ultrathin nanowires are used up by carbon dioxide molecules, and no methane molecules are produced
X. Li *et al.* (2012)[67]	HNb_3O_8/3.66 eV	Hydrothermal synthesis	CO_2 (saturated), water vapor (7 kPa)/350 W Xe lamp/—	(318/—/—/4/—), (0.1/39.4/1.12 nm particle/—/supported)	Methane/3.58/—	• KNb_3O_8 and HNb_3O_8 nanobelts show greater activities for CO_2 photoreduction to methane than commercial TiO_2, and the KNb_3O_8 and HNb_3O_8 particles synthesized by conventional solid-state reaction • The protonic acidity also gives higher photocatalytic activity to the HNb_3O_8 nanobelts • A fixed-bed quartz tubular reactor (159 mL) is placed horizontally, and the catalysts are put inside on a flat quartz plate
J. W. Lekse *et al.* (2012)[69]	$CuGaO_2$/2.6 eV	Stoichiometric mixing	CO_2 (saturated), water vapor (—)/300 W Xe arc lamp/—	(—/—/7/—/—), (0.2/—/60–80 mesh particles/—/supported)	Carbon monoxide/9[b]/—	• Alloying the B-site with Fe to form $CuGa_{1-x}Fe_xO_2$ ($x = 0.05, 0.10, 0.15, 0.20$) creates response toward visible and near-infrared regions • A gas-tight cell is built by stainless steel conflat flange components fitted with two inlet/outlet valves, and one UV quartz viewport
Stock and Dunn (2011)[68]	$LiNbO_3$/3.6 eV	Pulverized with a mortar and pestle to produce particles	CO_2 (30%), H_2O (10 mL)/natural sunlight or Hg lamp/64.2 mW cm^{-2}	(—/—/—/6/2), (—/—/1 μm particle/—/supported)	Formic acid/7.7[c]/—	• The $LiNbO_3$ is kept on a platen (1.26×10^{-5} m^2) above the water to give a gas–solid catalytic reaction • MgO doped $LiNbO_3$ gives an energy conversion efficiency of 0.72% is lower than that of 2.2% for $LiNbO_3$ • The ferroelectric material assistances carrier separation and gives an improved catalytic performance
Y. Zhou *et al.* (2011)[65]	Bi_2WO_6/2.69 eV	Solid state reaction and hydrothermal method	CO_2 (saturated), H_2O (1 mL)/300 W Xe arc lamp (>420 nm)/—	(298/—/—/5/—), (0.1/5.6/nanoplates of 9.5 nm thickness/—/supported)	Methane/1.1/—	• Bi_2WO_6 nanoplates display excessive potential in the application of visible light energy • Ultrathin geometry of the nanoplates helps charge carriers to move swiftly from the interior to the surface for photoreduction • Catalysts are evenly dispersed on the glass reactor with an area of 4.2 cm^2
N. M. Dimitrijevic *et al.* (2011)[53]	TiO_2 (Degussa P-25 Aeroxide)/3.08 eV	TiO_2 was left in D_2O in order to exchange bound water	CO_2 (saturated), water vapor (2.8 mmol)/100 W Hg lamp (365 nm)/11 mW cm^{-2}	(298/1/—/2.6/—), (0.01/55/nanoparticle/—/supported)	Methane/4[d]/—	• It is proposed that the two-electron and one-proton reactions are responsible for initial step in the reduction of CO_2 on the surface of TiO_2 • A closed reactor is used having a circular pot sample holder with a diameter of 1.8 cm

Table 1 (*Contd.*)

Researcher (year) and ref.	Catalyst/band gap energy	Catalyst treatment technique	Reactants (amount)/radiation source/light intensity	Operating variables (T/P/pH/t/QE), physical properties (W/SA/PS/SC/MP)	Major product/yield (μmol h^{-1} per g catalyst)/efficiency (%)	Comments
T. Yui *et al.* (2011)[52]	TiO_2 (Degussa P-25)/3.08 eV	Treated by calcination and washing	CO_2 (—), H_2O (1.5 mL)/500 W Hg arc lamp (>310 nm)/—	(278/—/4.1/5/—), (0.15/—/nanoparticle/ 0.1/suspended)	Carbon monoxide/ 0.35/—	• CH_4 was the main product in case of Pd–TiO_2, and CO formation is significantly reduced, compared with that on the pretreated TiO_2 • Isotope labeling specifies that CO_2 and CO_3^{2-} are the main carbon sources of the CH_4 production • Catalysts are kept in a round-shaped quartz vessel of 6 cm diameter
Q. Liu *et al.* (2010)[66]	Zn_2GeO_4/4.5 eV	Solvothermal method	CO_2 (—), water vapor (—)/UV light/—	(—/—/—/16/—), (—/28.27/nanoribbon of 7 nm thickness/—/ supported)	Methane/0.41/—	• Ultra-long and ultrathin geometry of the Zn_2GeO_4 nanoribbon shows high performance on photocatalytic activity • The rate of CH_4 production over the Zn_2GeO_4 nanoribbon could be significantly enhanced by loading of Pt
K. Koci *et al.* (2009)[48]	TiO_2 (anatase)/ 3.0 eV	Sol–gel process	CO_2 (—), NaOH (0.2 M, 100 mL solution)/8 W Hg lamp (254 nm)/1.41 mW cm^{-2}	(—/1.08/—/24/—), (0.1/ 106/14 nm nanoparticle/0.001/ suspended)	Methane/0.308/—	• A stirred batch annular reactor (380 cm^3) with quartz inner tube and stainless steel shell tube is used in this experiment • The yields is observed in such an order: $H_2 > CH_4 > CH_3OH \geq CO$
Y. Liu *et al.* (2009)[63]	$BiVO_4$ (monoclinic)/ 2.24 eV	Microwave assisted hydrothermal method	CO_2 (—), H_2O (100 mL)/300 W Xe arc lamp (>400 nm)/—	(273/1/—/1/—), (0.20/—/ nanoparticles/—/ suspended)	Ethanol/110/—	• Photocatalyst $BiVO_4$ exhibits visible-light response • Intense irradiation creates huge amount of C1 intermediate species anchored on the $BiVO_4$, which dimerizes to form ethanol • Catalysts are dispersed in water and magnetically stirred inside the reactor
L. Yuliati *et al.* (2008)[59]	Ga_2O_3 (Kishida chemicals)/4.7 eV	Cleaning at 13.3 kPa of oxygen atmosphere at 1073 K for 1 hour	CO_2 (200 μmol), CH_4 (200 μmol)/300 W Xe-lamp (220–300 nm)/9 mW cm^{-2}	(473/1/—/3/—), (0.2/2/—/—/supported)	Hydrogen, carbon monoxide/4.13, 1.8/—	• Supplementary thermal energy enhances the reaction between methane and carbon dioxide by stimulating the thermal-activation steps in the reaction mechanism • A closed quartz reactor (30 cm^3) where the catalysts are spread over a flat bottom of the reactor (14 cm^2)
Xia *et al.* (2007)[70]	TiO_2 (Degussa P-25)/3.08 eV	Calcined at 723 K for 2 h	CO_2 (1 μmol), water vapor (5 μmol)/15 W UV lamp (365 nm)/—	(298/—/7/5/—), (—/50/ nanoparticle/—/ supported)	Methane/15/—	• Appropriate amount of MWCNTs as supports for TiO_2 could extraordinarily advance the efficiency of the photocatalytic reaction • Catalysts are kept on a piece of transparent glass and then put into a homemade stainless steel reactor
C.-C. Lo *et al.* (2007)[62]	ZrO_2 (Prochem)/ 5.0 eV	ZrO_2 is immobilized by coated glass pellets	CO_2 (99.8%), H_2 (95%)/15 W near UV lamps (254 nm)/—	(316/1.1/—/2/—), (0.25/—/100 mesh powder/—/supported and immobilized)	Carbon monoxide/ 0.51/—	• A circulated, packed-bed photocatalytic reaction system is made from a quartz tube with 480 mm length and 22.5 mm inner diameter • One-site Langmuir–Hinshewood kinetic model is successfully fitted to simulate the photoreduction rate

Table 1 (*Contd.*)

Researcher (year) and ref.	Catalyst/band gap energy	Catalyst treatment technique	Reactants (amount)/radiation source/light intensity	Operating variables (T/P/pH/t/QE), physical properties (W/SA/PS/SC/MP)	Major product/yield (μmol h^{-1} per g catalyst)/efficiency (%)	Comments
S. S. Tan *et al.* (2006)[50]	TiO_2 (80% anatase and 20% rutile)/3.0 and 3.2 eV	Heated-up to 473 K in oven	CO_2 (saturated), water vapor (saturated)/1.6 W UV light (253.7 nm)/—	(298/1/—/48/—), (100/50/4 mm porous pellet/—/supported)	Methane/0.014/—	• A cylindrical quartz tube fixed-bed photocatalytic reactor having dimensions 300 mm (length) and 74 mm inner diameter is operated for 48 h continuously • A good reduction yield is attained as compared with immobilized catalysts through the thin-film technique and anchoring method
G. R. Dey *et al.* (2004)[56]	TiO_2 (anatase)/3.0 eV	Suspension of TiO_2 in presence of 0.5 M 2-propanol	CO_2 (—), H_2O (5 mL)/light (350 nm)/—	(298/1/—/10/—), (0.005/—/325 mesh powder/—/suspended)	Methane/6/—	• It is observed that surface-adsorbed and *in situ*-generated CO_2 are liable for methane formation through photoreduction by TiO_2 • In presence of saturated O_2, the methane yield is lower, compared with that in aerated system while CO_2 yield is developed • A quartz cell (16.5 mL) having a gas-purging inlet and a gas sampling port is used to run the photoreduction of CO_2
K. Teramura *et al.* (2004)[61]	MgO (Merck) and ZrO_2/7.0 eV and 5.0 eV	Hydrated, filtered and calcinated in air at 873 K for 3 h	CO_2 (150 μmol), CH_4 (50 μmol)/500 W ultra high pressure Hg lamp/—	(293/1/—/5/—), (0.3/110/100 mesh powder/—/supported)	Carbon monoxide/2.4 and 0.48 respectively/—	• It is found that the substrate-modified insulating material shows reasonable activity in CO_2 reduction • Catalysts are kept on a on the flat bottom of a quartz reactor (closed static system) with capacity 18.9 mL
A. H. Yahaya *et al.* (2004)[71]	NiO/—	—	CO_2 (saturated), deionized water (70 mL)/high photon flux monochromatic light (355 nm)/—	(—/—/7/1.5/—), (0.3/—/powder/—/suspended)	Methanol/393/—	• The formation of methanol from CO_2 is a reversible process and degrades the photocatalytic process to generate hydrogen and CO_2 again • A Pyrex cell with optical-grade quartz windows is used for photoreduction of CO_2 having 35 mm diameter and 120 mm length
S. Kaneco *et al.* (1999)[54]	TiO_2 (anatase)/3.0 eV	Pretreated by boiling in 1 M nitric acid and thoroughly rinsing	CO_2 (saturated), H_2O (5 mL)/990 W Xe lamp (>340 nm)/96 mW cm^{-2}	(308/88.82/3/5/—), (0.05/8.7/230 nm nanoparticle/0.01/suspended)	Formic acid/1.8/—	• Adding of acidic solutions rather than pure water is superior for formic acid production • Stainless steel vessel (557.5 mL) with a glass window is used to carry out the photoreduction of CO_2
S. Kaneco *et al.* (1997)[55]	TiO_2 (anatase)/3.0 eV	Purity 99.9% and treated by 1 M nitric acid with distilled-deionized water	CO_2 (saturated), H_2O (57.5 mL)/990 W Xe lamp (340 nm)/96 mW cm^{-2}	(293/64.15/—/30/—), (0.05/8.7/230 nm particle/—/suspended)	Formic acid/0.28/—	• There is no formation of gaseous reduction products, and formic acid is entirely found in the aqueous solution • The internal surface was completely covered by Teflon to prevent contamination from the stainless steel and its catalytic effect on reduction

Table 1 (*Contd.*)

Researcher (year) and ref.	Catalyst/band gap energy	Catalyst treatment technique	Reactants (amount)/radiation source/light intensity	Operating variables (T/P/pH/t/QE), physical properties (W/SA/PS/SC/MP)	Major product/yield (μmol h^{-1} per g catalyst)/efficiency (%)	Comments
M. Anpo *et al.* (1995)[72]	Anatase TiO_2 (JRC-TIO) and rutile TiO_2 (JRC-TIO)/3.47 and 3.32 eV	Degassed and calcined at 452 °C	CO_2 (0.15 mmol), water vapor (0.25 mmol)/75 W high-pressure Hg lamp (>280 nm)/—	(275/—/—/8/—), (—/16 and 51/1 μm finely powdered/—/ supported)	Methane/0.03 and 0.02 respectively/—	• The photocatalytic reactions are conducted in a quartz cell with a flat bottom (60 mL), where the catalysts are put on a transparent porous Vycor glass • TiO_2 (anatase) with large band gaps and many surface –OH groups exhibit high efficiency for the formation of CH_4
F. Solymosi and I. Tombacz (1994)[73]	TiO_2/—	Pure TiO_2 from British Drog House	CO_2 (saturated), H_2O (120 mL)/500 W high pressure Xe lamp/—	(333/1/—/—/—), (0.3/ 18/nanoparticle/0.0025/ suspended)	Formic acid/2/—	• A Pyrex glass cell with a Pyrex window is used to conduct the photocatalytic reaction having surrounding water jacket to control the temperature of circulating water by an ultra-thermostat • An increase in the electron concentration of TiO_2 enhances the photoreduction
T. Inoue *et al.* (1979)[42]	TiO_2, ZnO, and WO_3/3.0, 3.2, and 2.8 eV	Purity 99.5 to 99.99%	CO_2 (saturated), H_2O (100 mL)/500 W Xe or Hg lamp/—	(298/1/5/7/—), (1/—/ 200–400 mesh powder/—/suspended)	Formaldehyde/16, 17.14, and 0/—	• Methanol formation rate is increased by increasing illumination period in case of TiO_2 • In case of semiconductor electrode, it has been suggested that the charge transfer rate between photogenerated carriers and solution species is related to the energy levels between the semiconductor and redox agents • A glass cell with quartz window is used to carry out the reaction

[a] T/P/pH/t/QE: temperature (K)/pressure (atm)/pH/illumination period (hours)/quantum efficiency (%). W/SA/PS/SC/MP: weight of photocatalyst (g)/surface area (m^2 g^{-1})/photocatalyst structure (diameter)/semiconductor concentration (g mL^{-1})/mode of photocatalyst. '—': not mentioned in the original paper. [b] ppm h^{-1} g^{-1} catalyst. [c] mmol h^{-1}. [d] Turn over number.

of 2.7 eV for the photocatalytic conversion of CO_2 to methane under visible light irradiation.[58] The diameter of $W_{18}O_{49}$ nanowires is approximately 0.9 nm and hold a large number of oxygen vacancies. These oxygen vacancies indicate an outstanding competency on photochemical carbon dioxide reduction over the visible light region.

Metal oxides like Ga_2O_3, ZrO_2, and MgO were reported in various studies as having wide band gaps, compared with other photocatalytic metal oxides.[59–61] In those studies, methane and hydrogen were used as reductants for photoreduction of CO_2, and CO was the major product.[61,62] In the case of ZrO_2, high photoreduction of CO_2 is obtained when H_2 is used rather than CH_4. Moreover, it is found that some intermediates are formed when H_2 is used for CO_2 photoreduction over ZrO_2 and MgO as a surface formate species, whereas the acetate is generated *in lieu* of the formate when CH_4 is used as reductant over ZrO_2.[60,61] It was also observed that the surface bidentate formate species showed high photoactivity for photocatalytic reduction of CO_2 over ZrO_2 and MgO.

Recently, visible light-responsive and other oxide catalysts fabricated through various routes like hydrothermal, solvothermal, and solid state reactions are widely used in the photochemical reduction of CO_2 because of high yield rates. Microwave-assisted, hydrothermally derived monoclinic $BiVO_4$ catalysts show higher ethanol yields (110 μmol h^{-1} per g of catalyst) than that of tetragonal $BiVO_4$ due to anchored CO_3^{2-} to the Bi^{3+} sites on the external surface through a weak Bi–O bond for receiving the photogenerated electrons effectively from the V 3d-block bands of $BiVO_4$. The asymmetric behavior of the monoclinic phase around the Bi^{3+} ion is more effective than in the tetragonal phase. That is why, the Bi^{3+} ion shows a stronger lone pair behavior in the monoclinic phase for increasing the tendency of the Bi–O bond formation with CO_3^{2-}.[63,64] Y. Zhou *et al.* and Q. Liu *et al.* reported visible light-responsive, 9.5 nm thick Bi_2WO_6 nanoplates and UV-driven single-crystalline Zn_2GeO_4 nanobelts with a thickness of 7 nm, respectively.[65,66] The ultrathin geometry encourages the charge carriers to transfer swiftly from inside to the external surface for effective participation in the CO_2 photoreduction reaction. It also separates the photogenerated electron and hole progressively, ultimately decreasing the recombination rate.

It has been reported that hydrothermally prepared KNb_3O_8 and HNb_3O_8 nanobelts show high yields of methane, compared with the same catalysts derived from conventional solid state reactions and commercial TiO_2 (Degussa P25).[67] In the case of hydrothermal synthesis, this nanobelt-like morphology and protonic acidity give higher photochemical activity for methane production through hydrogen bonding, which is facilitated by the separating and trapping of photogenerated carriers at the interlayer surfaces of HNb_3O_8 and KNb_3O_8. Ferroelectric materials can be used as remarkable substitutes for the standard semiconductor photocatalysts. Ferroelectric characteristics lead to driving the electrons and holes apart because they possess internal dipoles. Therefore, this phenomenon decreases the probabilities of the recombination of carriers and also inhibits the reaction of redox products, driving the equilibrium towards product formation. For this ferroelectric behavior, the polar compound $LiNbO_3$ was used by Stock and Dunn for photocatalytic CO_2 conversion to formic acid under an Hg lamp or direct natural sunlight irradiation.[68]

2.1.2 Supported metal oxide photocatalysts. Several types of supportive materials were used in this technology, such as zeolite, mesoporous SiO_2, kaolinite, Al_2O_3, montmorillonite and other pillar materials. Table 2 demonstrates the textural belongings of the silica supports and the TiO_2-loaded samples with specific surface area, pore volume, and maximum pore size distributions.[46] The mesoporous, SiO_2-prepared material MCM-41 shows higher specific surface area having an average pore size of 2.3 nm. The pore structure of supported materials is a vital factor because it manages the transportation of reactants and products to and from the surface, and controls the size of the active surface area.[74] The detailed information of supported metal oxide semiconductors investigated in previous studies are highlighted critically in Table 3. Titania charging on the silica matrix reduces the surface area of the supports and also decreases the pore volume, as the titania content increases. The reduction of pore volume indicates that the loading of semiconductor particles saturates the maximum space of the ordered channels within the support, which helps to control the catalysts' size from crystal growth. High catalyst loading can cause pore blockage inside the channels, although the interconnection among the parallel pore channels should have the ability to reduce this effect.[75] The common photocatalytic reaction path for supported metal oxide semiconductor is illustrated in Scheme 1(b).

A catalyst on supported materials has been used in many photocatalytic aqueous systems due to their immobilization in terms of easier separation of the catalyst after the photocatalytic reactions. It is reported that supported photocatalysts exhibit lower activities than powdered TiO_2 materials. However, treated photocatalysts show their high activity because of cyanide content and represent the dicyanoaurate photoreduction activity in order to reflect $TiO_2/GrSiO_2$ > Degussa P25 > TiO_2/SBA-15. Depending on the treatment processes, TiO_2/SBA-15 materials achieved up to eight times of high activity, compared with the Degussa P25 TiO_2.[76] The addition of Cu species on TiO_2–SiO_2 catalysts increased the overall CO_2 conversion efficiency by suppressing the electron–hole recombination and increasing multi-electron reactions,[77] compared with only TiO_2–SiO_2 matrices.[78] It is reported that the addition of 0.5% Cu shows high specific surface area, but the addition of 1% and 3% Cu successively reduces the specific surface area. A multi-walled carbon nanotube (MWCNT)-supported TiO_2 composite catalyst is introduced by Xia *et al.* due to its unique electronic properties,[70] and the results show a high conversion rate when a proper amount of MWCNTs is used as a support for TiO_2. Moreover, the MWCNT-supported composite catalysts are able to lessen the accumulation of the catalyst particles and reduce the recombination of electron–hole pairs by moving it along the tubes. Carbon is used as a catalyst support in gas–solid reaction phases with suitable temperature and pressure under which the carbon support remains stable. In hydrogenation reactions, carbon-supported iron catalysts with high dispersions were used at 1 atm and <700 K because of carbon stability under this

Table 2 Textural properties of different types of silica-supported samples[46]

Catalysts' composition	Specific surface area ($m^2\ g^{-1}$)	Pore volume ($cm^3\ g^{-1}$)	Maximum of the pore size distribution (nm)
MCM-41 SiO_2	1051	0.83	2.3
SBA-15 SiO_2	640	0.96	7.5
SBA-15/TMB SiO_2	601	1.62	20.0
Commercial SiO_2	317	1.59	27.5
100% TiO_2 reference	9	—	—
20% TiO_2 MCM-41	294	0.57	16.0
20% TiO_2 SBA-15	532	0.78	7.0
40% TiO_2 SBA-15	442	0.69	6.5
60% TiO_2 SBA-15	349	0.60	6.5
20% TiO_2 SBA-15/TMB	517	1.40	18.5
40% TiO_2 SBA-15/TMB	414	1.08	18.5
60% TiO_2 SBA-15/TMB	304	0.78	18.5
20% TiO_2 commercial	299	1.16	22.5
40% TiO_2 commercial	246	0.94	25.0
60% TiO_2 commercial	179	0.67	26.0

condition.[74] The stability of activated carbon can be controlled by ZnO catalysts. The high reaction rate of the gasification of the activated carbon is carried out with CO_2 by ZnO loading in low temperatures.[79] The presence of an acidic medium in mixed oxide systems is suitable to achieve additional knowledge on the physical nature of photocatalysts.[80] The oxide-supported catalysts are treated by an acidic medium due to the presence of an oxygen species in the reaction system that leads to a formation of basic nature of the catalyst, which was reported by M. Subrahmanyam *et al.*[81] Zeolites are microporous, aluminosilicateminerals having porous structures as traps for molecules to analyze. Investigation shows that the TiO_2 particles are highly distributed inside the pore channels of zeolite with tetrahedral coordination, which has high selectivity for the formation of CH_3OH.[82] At the same time, it was also found that Pt loading on TiO_2 catalysts in the presence of zeolite support encourages the charge separation and increases the formation of CH_4 *in lieu* of CH_3OH by stimulating the reaction between the carbon radicals and H atoms formed on the Pt metals to produce CH_4.

Recently, montmorillonite has been loaded with TiO_2 structures to increase the surface area of TiO_2 particles.[45] Ultimately, in this research, the particle size of the catalyst was reduced from 18.73 to 13.87 nm and allowed efficient charge separation. The band gap of TiO_2 was also reduced to 3.07 eV and could permit visible light irradiation during photoreduction of CO_2 in the presence of water vapor. Effective charge transfer between the two semiconductors and the response to visible light are found in the $FeTiO_3$–TiO_2 catalyst due to its unique band structure (2.7 eV).[83] When the loading of $FeTiO_3$ increases on TiO_2 from 10% to 50%, it shows a decrease in surface area accordingly from 55.8 to 35.7 $m^2\ g^{-1}$. Due to the small surface area, a high content of $FeTiO_3$ on TiO_2 provides a low production rate. Kaolinite, which is a clay mineral with a layered silicate having one tetrahedral sheet connected through oxygen atoms to one octahedral sheet of alumina octahedral,[84] is another promising supporting material in this technology. A kaolinite/TiO_2 composite decreases the crystallite size of anatase TiO_2. Kaolinite increases the effective surface area for TiO_2 by avoiding TiO_2 aggregates in suspension and prevents the recombination of electron–hole pairs. It also hinders crystallite growth and decreases particle sizes from 26 nm to 18 nm.[85] 23.2% AgBr is highly dispersed on the surface of TiO_2 nanoparticles, which exhibit strong absorption ability in the visible-light region and stability during repeated operations because of transferring photoexcited electrons from conduction bands of well-dispersed AgBr to that of TiO_2.[86] RuO_2 is a favorable material which shows high electrical conductivity and electrochemical stability, intermediate hydrogen over-potential and the capacity to reversibly adsorb hydrogen for CO_2 reduction.[87] RuO_2 supported on TiO_2 nanotube-composite-modified Pt electrodes showed higher activity on electrochemical reduction of CO_2 to methanol, compared with RuO_2-modified Pt electrodes, according to the investigation of J. Qu *et al.*[88] It is also found that RuO_2–TiO_2 nanotube-modified electrodes are more promising electrocatalysts than that of RuO_2–TiO_2 nanoparticle-modified electrodes due to the high dispersion of RuO_2 on the TiO_2 nanotubes surface with more surface area, creating more active sites. Photoreduction rates can be improved by the deposition of Pd metal on the surface of RuO_2–TiO_2, where photoelectrons are trapped by Pd, and photoholes are confined at the RuO_2/SO_3^{2-} site.[89] WO_3 and CeO_2 were also applied on TiO_2 support to investigate photocatalytic activity,[73,90] where CeO_2–TiO_2 shows the visible light responsiveness. The loading of Rh on TiO_2 containing 2% WO_3 leads to the formation of more formic acid, compared with WO_3–TiO_2.[73]

Some other investigations were published based on the CuO, which is highly dispersed on TiO_2.[91,92] By using XRD analysis, it is found that the dispersion capability of CuO in the vacant sites of TiO_2 was approximately 4.16 $Cu^{2+}\ nm^{-2}$. The high percentage of CuO loading on TiO_2 slightly reduces the surface area of catalyst particles, and this slight change in surface area is negligible to the reactivity of the catalyst.[91] On the other hand, 1 wt% CuO–TiO_2 exhibits high band gap energy (3.02 eV) with lower production yields than that of 3 wt% CuO–TiO_2 (2.88 eV).[91] Calcination temperature is also important in terms of production

Table 3 Advances in supported metal oxide catalyst for CO_2 photoreduction[a]

Researcher (year) and ref.	Catalyst composition/ band gap energy	Catalyst preparation technique	Reactants (amount)/radiation source/light intensity	Operating variables (T/P/pH/t/QE), physical properties (W/SA/PS/SC/MP)	Major product/yield (μmol h^{-1} per g catalyst)/selectivity (%)	Comments
M. Tahir *et al.* (2013)[45]	20 wt% montmorillonite modified TiO_2/ 3.07 eV	Sol–gel method	CO_2 (saturated), water vapor (—)/500 W Hg lamp (365 nm)/—	(393/0.20/—/4/—), (0.05/82.62/13.87 nm particle/6.33/ supported)	Methane/441.5/—	• Loading montmorillonite onto TiO_2 structure amplified surface area, reduced particle size and allowed efficient charge separation • H_2O/CO_2 feed ratio = 0.35 gives the maximum yield for methane (441.5 μmol g cat^{-1} h^{-1}) • Stainless steel reactor having length of 9.5 cm, width of 3.75 cm and total volume of 106 cm^3 with a quartz window for the passing of light irradiations
Q. D. Truong *et al.* (2012)[83]	20% $FeTiO_3$–TiO_2/2.7 eV	Facile hydrothermal method	CO_2 (—), $NaHCO_3$ (0.08 M, 30 mL solution)/500 W Xe lamp (>300 nm)/—	(—/—/—/3/—), (0.05/ 51.3/5 nm particle/—/ suspended)	Methanol/0.46/—	• Junction effect of two semiconductors and narrow band gap of $FeTiO_3$ show extraordinary activity under both visible and UV-vis light irradiation with a supreme yield of CH_3OH that is three times higher than that from bare TiO_2 or Degussa P25 • A Pyrex glass tube reactor where the temperature of the solution is kept constant by a water bath
D.-S. Lee *et al.* (2012)[95]	1 wt% NiO–$InNbO_4$/—	Solid-state reaction and wetness impregnation methods	CO_2 (saturated), $KHCO_3$ (0.2 M, 50 mL solution)/500 W halogen lamp (900 nm)/143 mW cm^{-2}	(298/—/7/20/—), (0.14/—/1 μm particle/—/dispersed and suspended)	Methanol/1.4/—	• Catalyst shows highest activity due to the presence of core–shell type Ni^0 and NiO on the surface and the presence of a small amount of Nb_2O_5 as a promoter under visible light irradiation • Photocatalytic reduction is carried out in a continuous flow reactor with a Pyrex glass down-window type irradiation cell (75 mL)
Q. Liu *et al.* (2012)[99]	1 wt% Pt and 1 wt% RuO_2 loaded on $Zn_{1.7}GeN_{1.8}O$/2.6 eV	Solvothermal route and nitridation	CO_2 (saturated), H_2O (0.4 mL)/300 W Xe arc lamp (>420 nm)/—	(298/1/—/14/0.024), (0.1/32.33/0.5–2 μm bundle shape/—/ supported)	Methane/11.5/—	• This hybrid photocatalyst allows CO_2 reduction into CH_4 in the presence of H_2O under visible light irradiation • Photocatalysts are evenly put at the bottom of a Pyrex glass reactor with an area of 4.2 cm^2
K. Kočí *et al.* (2011)[85]	Kaolinite modified TiO_2 composite/—	Thermal hydrolysis	CO_2 (saturated), NaOH (0.2 M, 100 mL solution)/8 W Hg lamps (254 nm)/—	(—/1/7/24/—), (1/40/18 nm particle/0.001/ supported)	Hydrogen/0.187/—	• Production of methane and methanol were advanced over a kaolinite-modified TiO_2 composite than over commercial TiO_2 (Degussa P-25) • Adding of TiO_2 nanoparticles into the kaolinite structure caused a decrease of anatase crystallite size • Inhibit the recombination of electron–hole pairs and stop the formation of TiO_2 aggregates in suspension • The photocatalytic reduction is conducted in a homemade apparatus using a stirred batch annular reactor with a suspended catalyst

Table 3 (*Contd.*)

Researcher (year) and ref.	Catalyst composition/ band gap energy	Catalyst preparation technique	Reactants (amount)/radiation source/light intensity	Operating variables (T/P/pH/t/QE), physical properties (W/SA/PS/SC/MP)	Major product/yield ($\mu mol\ h^{-1}$ per g catalyst)/selectivity (%)	Comments
M. A. Asi *et al.* (2011)[86]	23.2 wt% AgBr–TiO_2/2.9 eV	Deposition–precipitation method	CO_2 (saturated), $KHCO_3$ (0.2 M, 100 mL solution)/150 W Xe lamp (420 nm)/—	(298/74/8.5/5/—), (0.5/50/5 nm particle/—/suspended)	Methane, ethanol/25.72, 15.57/—	• AgBr–TiO_2 shows its strong absorption and stability in the repeated uses under visible-light region due to the transmission of photoexcited electrons from the conduction band of well-dispersed AgBr to that of TiO_2 • Photocatalytic reduction is conducted in a stainless steel vessel with valves for evacuation and gas feeding in which an O-ring sealed glass window is kept at the top for focusing light
P.-Y. Liou *et al.* (2011)[93]	1 wt% NiO–$InTaO_4$/2.6 eV	Impregnation method	CO_2 (saturated), water vapor/300 W Xe lamp/100 mW cm^{-2}	(303/1/—/6/0.057), (0.12/3.58/composite/—/supported)	Acetaldehyde/0.3/—	• To increase the amount of catalyst loading, a monolith photoreactor is used due to its multiple channels • Surface-carved polymethylmethacrylate optical fibers can transmit and scatter light effectively to illuminate the catalyst inside the channels • Quantum efficiency was significantly enhanced in the monolith reactor, compared with the optical-fiber reactor
S. Yan *et al.* (2011)[98]	3 wt% RuO_2–Zn_2GeO_4/4.65 eV	Low-temperature (100 °C) solution phase route	CO_2 (saturated), H_2O (—)/ultra-violet irradiation/—	(—/—/—/5/—), (—/14.8/rod-shaped nanostructure/0.58/supported)	Carbon monoxide/17.9[b]/—	• Facile solution phase route-synthesized catalysts have low crystal defects, high specific surface area and beneficial microstructure on its surface
S. Qin *et al.* (2011)[92]	1 wt% CuO–TiO_2/3.2 eV	Laboratory synthesis	CO_2 (saturated), methanol (30 mL solution)/250 W high pressure Hg lamp (365 nm)/—	(300/1–60/—/6/—), (0.03/—/13.8 nm particle/—/suspended)	Methyl-formate/1602/—	• Methanol acts as a sacrificial reagent to react with the photogenerated holes in the valence band • Hetero-junction photocatalyst reduces the recombination of the electrons and holes • The photocatalytic reaction is conducted in a slurry reactor having a flat top cover of the vessel is made of Pyrex glass
Ying Li *et al.* (2010)[77]	SiO_2 supported 0.5 wt% Cu–TiO_2/3.1 eV	One-pot sol–gel method	CO_2 (saturated), water vapor (—)/Xe lamp (250–400 nm)/2.4 mW cm^{-2}	(273/1/7/4/1.41), (0.1/386.2/<100 μm powder/—/supported)	Carbon monoxide/45/—	• Experiment is carried out in a continuous-flow reactor having stainless steel wall with a quartz window at the top, and the inner cavity is 6.0 cm in diameter and 2.5 cm deep • High surface area of mesoporous silica substrate significantly improves CO_2 photoreduction because of improved TiO_2 dispersion and high CO_2 and H_2O adsorption on the catalyst • Cu species suppress the electron–hole recombination and enhancing multi-electron reactions

Table 3 (*Contd.*)

Researcher (year) and ref.	Catalyst composition/ band gap energy	Catalyst preparation technique	Reactants (amount)/radiation source/light intensity	Operating variables (T/P/pH/t/QE), physical properties (W/SA/PS/SC/MP)	Major product/yield (μmol h^{-1} per g catalyst)/selectivity (%)	Comments
X.-H. Xia *et al.* (2007)[70]	TiO_2–MWCNT/—	Sol–gel and hydrothermal methods	CO_2 (1 mol), water vapor (5 mol)/15 W UV lamp (365 nm)/—	(298/—/7/5/—), (0.1/50/ nanoparticle/—/ supported)	Ethanol, formic acid/30, 19/—	• Catalyst is placed over a piece of transparent glass and then laid into a homemade stainless steel reactor • MWCNTs in the composite catalysts can mitigate the accumulation of TiO_2 particles and decrease the recombination of electron–hole pairs • MWCNTs have enhanced performance in the photocatalytic reactions as supports for TiO_2, compared with activated carbons
P.-W. Pan and Y.-W. Chen (2007)[94]	1.0 wt% NiO–$InTaO_4$/2.6 eV	Solid state reaction and wet impregnation method	CO_2 (saturated), $KHCO_3$ (0.2 M aqueous solution)/ 500 W halogen lamp (365 nm)/—	(298/—/—/20/—), (0.14/—/1–2 μm particles and pellets/—/ suspended)	Methanol/1.4/—	• Continuous mode down-window-type irradiation cell reactor made of Pyrex glass (75 mL) is used to carry out the photoreaction • The methanol yield increases with the amount of NiO co-catalyst • Catalysts have ability to reduce CO_2 to methanol under visible light illumination
J. Qu *et al.* (2005)[88]	RuO_2–TiO_2 nanotube modified Pt electrode/—	Sol–gel method and laboratory synthesis	CO_2 (saturated), $NaHCO_3$ (0.5 M, 50 mL solution)/ electrochemical reduction/—	(298/—/—/—/current efficiency 60.5[c]), (0.001/—/25 nm nanoparticle composite electrode/—/supported)	Methanol/—/—	• High efficiency and selectivity for electrochemical reduction of CO_2 depends on the surface structure of the nanotubes composite electrode • Experiments are done in a standard three-electrode electrochemical cell where a saturated calomel electrode is used as the reference electrode
Nasution *et al.* (2005)[91]	3% CuO–TiO_2/ 2.88 eV	Improved impregnation method	CO_2 (saturated), $KHCO_3$ (1 M, 300 mL solution)/10 W UV black light lamp (415–700 nm)/2.45 mW cm^{-2}	(333/—/—/6/19.23), (0.3/45.8/23 nm particle/—/suspended)	Methanol/442.5/19.23	• Slurry type photocatalytic reactor consists of a horizontal stainless steel vessel with an inner diameter and height of the vessel 140 and 50 mm, respectively having a plate cover at the top of the vessel is made of Pyrex • The positive values of E_a indicate that desorption of products is the rate-limiting step in the photosynthetic formation of methanol
N. Gokon *et al.* (2003)[79]	5 wt% ZnO on activated carbon/ 3.2 eV	Impregnation method	CO_2 (saturated), —/Xe lamp (<400 nm)/34000 mW cm^{-2}	(873/—/—/—/—), (0.10/—/150–300 mm particle/—/supported)	Carbon monoxide/2 × 10^5/—	• Sample is kept in quartz tube reactor (8 mm diameter) is supported from both sides by alumina honeycomb covered with quartz wool and irradiated by a solar furnace simulator • This is a high-temperature operation for photocatalytic conversion of CO_2
T.-F. Xie *et al.* (2001)[89]	Pd–RuO_2 supported on TiO_2/—	Laboratory synthesis	CO_2 (saturated), NaOH with Na_2SO_3 (0.05 M)/450 W Xe short-arc lamp/—	(298/1/—/—/—), (0.02/—/22 nm particle/—/suspended)	Formate/72.3[c]/—	• Surface noble metal (Pd and Ru) deposition is a costly and economically unfeasible for industrial purposes • Reaction is carried out in a 30 mL Pyrex glass cuvette and stirred continuously by a magnetic stirring bar

Table 3 (*Contd.*)

Researcher (year) and ref.	Catalyst composition/ band gap energy	Catalyst preparation technique	Reactants (amount)/radiation source/light intensity	Operating variables (T/P/pH/t/QE), physical properties (W/SA/PS/SC/MP)	Major product/yield (μmol h^{-1} per g catalyst)/selectivity (%)	Comments
M. Subrahmanyam *et al.* (1999)[81]	10 wt% TiO_2–Pd supported on Al_2O_3/—	Impregnation method	CO_2 (saturated), $KHCO_3$ (0.5 M solution)/0.25 W Hg arc lamp/—	(—/—/7.5/6/—), (—/—/Particle/—/ suspended)	Acetone/8.5[d]/—	• The experiment is conducted in a well-mixed heterogeneous batch type reactor • Catalyst on support accomplishes the condition of a good photocatalyst to produce C1 and C2 compounds
B.-J. Liu *et al.* (1998)[78]	TiO_2– SiO_2 matrices/—	Sol–gel method	CO_2 (saturated), lithium nitrate and propan-2-ol (20 and 1 mmol dm^{-3})/500 W Hg arc lamp (280 nm)/1000 mW cm^{-2}	(—/—/—/8/0.16), (—/290/5.3 nm spherical particle/3.89/ supported)	Formate/0.5[d]/—	• It is decided that reduction reaction of nitrate ions is the rate-determining step of the formation of urea • The photoreduction is carried out using a quartz cell (9 cm^3), whose top is sealed with a rubber septum and the transparent TiO_2–SiO_2 film coated on a quartz plate (2 cm^2) was vertically submerged in solutions
M. Anpo *et al.* (1997)[82]	1.1 wt% TiO_2 – Y zeolite cavities/—	Ion-exchange method	CO_2 (24 μmol), water vapor (120 μmol)/75 W high-pressure Hg lamp (>280 nm)/—	(328/1.31x 10^{-9}/—/6/—), (0.15/—/powder/—/ supported)	Methanol/5/—	• Based on Ti^{3+}, H atoms and C radicals, a molecular–scale reaction mechanism has been proposed • Highly dispersed isolated tetrahedral titanium oxide species deliberate the active sites for reaction systems
Solymosi *et al.* (1994)[73]	2% WO_3–TiO_2/—	Wet impregnation method	CO_2 (saturated), H_2O (120 mL)/500 W high pressure Xe lamp/0.68 mW cm^{-2}	(333/1/—/5/—), (0.3/18/ nanoparticle/0.0025/ suspended)	Formic acid/1.4/—	• Reaction is carried out in a Pyrex glass cell where the reaction temperature is controlled by a surrounding water jacket in which the temperature of circulating water is regulated by an ultra-thermostat
K. Ogura *et al.* (1992)[90]	0.5 wt% CeO_2–TiO_2/—	Heating co-precipitation	CO_2 (0.13 atm), H_2O (0.032 atm)/500 W Xe lamp (<370 nm)/—	(298/1/—/18/—), (1/111/ nanoparticle/—/ suspended)	Hydrogen/0.26/—	• Photocatalytic reaction is performed in an apparatus of closed circulating system (1.5 dm^3) and visible light irradiation is applied from the bottom *via* a rectangular quartz prism

[a] T/P/pH/t/QE: temperature (K)/pressure (atm)/pH/illumination period (hours)/quantum efficiency (%). W/SA/PS/SC/MP: weight of photocatalyst (g)/surface area (m^2 g^{-1})/photocatalyst structure (diameter)/semiconductor concentration (g mL^{-1})/mode of photocatalyst. '—': not mentioned in the original paper. [b] ppm h^{-1}. [c] ppm. [d] μmol h^{-1}.

rates. 1 wt% CuO–TiO_2 calcined at 450 °C represents greater activity than that of calcined at 350 °C and 550 °C.[92]

In addition, supported materials other than TiO_2 are found at reasonable photocatalytic activity. The use of NiO on several metal oxides such as $InTaO_4$ and $InNbO_4$ are found in some publications for CO_2 reduction to fuel.[93–95] 1 wt% NiO–$InTaO_4$ catalysts have low band gap energy of 2.6 eV, which is highly responsive to visible light and can be used in different types of reactors like slurry, optical fiber and monolithreactors.[93,96,97] In case of NiO–$InNbO_4$ catalyst, it shows also better activity due to the presence of core–shell-type Ni^0 and NiO on the surface and the presence of a small amount of Nb_2O_5 as a promoter under visible light irradiation.[95]

Zn_2GeO_4 is an important metal oxide catalyst in photoconversion technology, which is frequently used as a support for other oxide catalysts to enhance photocatalytic CO_2 conversion. Zn_2GeO_4 catalyst contains some superior properties like low crystal defects, extraordinary specific surface area and favorable microstructure on the surface of the catalyst, but the band gap energy is high enough (4.65 eV) to show the visible light response.[98] Sheaf-like, hyperbranched Zn_2GeO_4 nanoarchitecture was developed by Q. Liu *et al.*, which was further modified by NH_3 flow to a yellow $Zn_{1.7}GeN_{1.8}O$ solid solution for CO_2 conversion into carbonaceous fuel in the existence of water at ambient conditions under visible light irradiation.[99] The modified catalyst shows low band gap energy (2.6 eV), which is used as a support for 1 wt% Pt and 1 wt% RuO_2. Moreover, the loading of Pt and RuO_2 on $Zn_{1.7}GeN_{1.8}O$ gives a high conversion rate, which is able to arrest the electron–hole pairs by preventing the recombination of electrons and holes.

2.2 Modified/unmodified non-oxide catalysts

Non-oxide semiconductor photocatalysts are selected for CO_2 recycling because of their low band gap energy to facilitate the photocatalytic response to the visible light region, and high conversion efficiency is achieved for their unique photobehavior. Elaborately major findings and characteristics of non-oxide semiconductors upon photocatalytic reactions are described in Table 4.

2.2.1 Metal sulphide semiconductors. It is investigated that semiconductor catalysts are one of the supreme sources for direct solar energy conversion. Many wide-ranging reviews already have been published on the advancement of oxide or non-oxide semiconductor photoactive materials.[100–103] It was found that apart from the metal oxide semiconductor catalysts, metal sulphide semiconductor materials have effective photoactivity because of their outstanding ability to absorb the solar spectrum with high energy yields.[104] Metal sulphides have comparatively high conduction band states more appropriate for enhanced solar responses than for metal oxide semiconductors, which are facilitated by the higher valence band states consisting of S 3p orbitals.[104] It was reported that to absorb the entire UV and visible light region of solar irradiation, a ZnS–$AgInS_2$–$CuInS_2$ solid solution was capable due to an absorption edge of up to 800 nm.[105] Fujiwara *et al.* investigated ZnS–DMF(OAc) for the CO_2 photoreduction process.[106] They found that the close interaction of acetate ions to Zn atoms inhibited the creation of sulfur vacancies as catalytic sites for CO production. Moreover, surface dimethylformamide (DMF) solvated Zn atoms give more efficiency to $HCOO^-$ formation. On the other hand, the addition of excess Zn^{2+} increases the size of ZnS–DMF(OAc) through the reaction between excess Zn^{2+} and the surface of ZnS–DMF(OAc) nanocrystallites. ZnS deposited on montmorillonite (MMT) was also fabricated by Kočí *et al.* with particle sizes of 3 nm to 5 nm, which provided significantly higher productivity, compared with the commercial TiO_2 Degussa P25.[107,108] They used cetyltrimethylammonium (CTA) with ZnS nanoparticles to inhibit the formation of bigger agglomerates. Different percentages of ZnS loading on porous SiO_2 matrices were also applied to investigate the improved photocatalytic yields.[109]

In 1979, Inoue *et al.* introduced non-oxide semiconductor catalysts (CdS, GaP and SiC) for the photocatalytic conversion of CO_2 to fuel.[42] Among them, CdS shows comparatively better yields in CO_2 conversion. It is found from Table 4 that the narrow band gap (2.63 eV) CdS supported on montmorillonite exhibits a lower conversion yield than that of 3.89 eV ZnS deposited on MMT, but the CdS–MMT system has high stability in presence of CTA.[108,110,111] Not only that, here CTA acts as a binder among CdS and MMT particles. Photocatalytic conversion of CO_2 on CdS semiconductors with modified surfaces by various types of thiol compounds was performed in presence of 2-propanol solvent.[112] In this study, the major products found were formate and carbon monoxide. The ratio of formate to carbon monoxide is highly dependent on the solvent and increases with increasing the dielectric constant of the solvent. Moreover, the surface modifier is used in this system to fix the surface Cd^{2+} sites, thus decreases the adsorption of $CO_2^{\bullet-}$ on Cd^{2+} sites, which means that the formate yield will be increase with increasing the surface exposure of the modifier. Another study shows that extra Cd^{2+} addition to the CdS–DMF system forms sulfur vacancies on the surface of nanocrystallites because of the adsorption of excess Cd^{2+} on the surface.[113] Over the surface of sulfur vacancies, CO_2 takes electrons sequentially after developing a $Cd^{2+}OCOCO_2$ complex to react with another CO_2, leading to the formation of CO as reported in the electrical CO_2 reduction to CO.[114]

Yuan *et al.* investigated CdS–TNT loaded with Pt to carry out the photochemical reaction under visible light irradiation, but they found that the worsening effect of photochemical reaction occurs due to the adsorption of intermediate products (CO, O_2 *etc.*) on Pt and the oxidation of Pt.[115] Another approach was led by Li *et al.* for visible light-responsive photocatalytic CO_2 reduction on modified CdS with 15% Bi_2S_3.[116] The investigation shows that the Bi_2S_3 catalyst itself has higher photochemical activity and visible light response than that of CdS. The addition of Bi_2S_3 increased the photochemical performance of CdS, and a maximum yield was obtained 120 μmol h^{-1} g^{-1} catalyst. Cd–ZnS was investigated to compare the photocatalytic behavior with solid solutions of ZnS–CdS microcrystals.[117] Cd–ZnS shows the highest activity than that of ZnS–CdS because Cd is more active in improving the quantum efficiency of the photochemical reduction of formate due to its ability to activate CO_2 more

Table 4 Advances in modified/unmodified non-oxide catalysts for CO_2 photoreduction[a]

Researcher (year) and ref.	Catalyst/band gap energy	Catalyst treatment/preparation technique	Reactants (amount)/ radiation source/ light intensity	Operating conditions (T/P/pH/t/QE), operating variables (W/SA/PS/SC/MP)	Major product/yield (μmol h^{-1} per g catalyst)/ efficiency (%)	Comments
K. Koci *et al.* (2011)[108]	ZnS deposited on MMT/3.89 ± 0.03 eV	Na_2S, CTA and $Zn(AcO)_2$ mixing by vigorous stirring	CO_2(saturated), NaOH (0.2M solution)/8 W Hg lamp (254 nm)/—	(273/1/—/24/—), (0.1/—/nanocomposite/ 0.001/suspended)	Methanol, methane/1.41, 1.33/—	• It is analyzed that product yields depend on the reactor diameter and on the volume of the liquid phase • Slurry-type two-stirred batch annular reactors is used with three quartz glass tubes of different diameters (3.5, 4.0 and 4.5 cm) placed inside the reactors • Perfect mixing is one of the most important factors in slurry reactors, and this mixing is difficult in annular reactors
J. Yuan *et al.* (2011)[115]	Pt loaded on CdS–TNT/—	Alkaline hydrothermal method and immersing TNT in $Cd(CH_3COO)_2$ with heat treatment	CO_2 (5000 ppm), water vapor (—)/UV-vis and visible light irradiation/—	(298/—/—/6/—), (—/—/nanotube/—/ supported)	Methane/7800[c]/—	• Adsorption of intermediate products (CO, O_2) on Pt, and the oxidation of Pt might be the reasons for the deterioration of photocatalytic reaction
P. Praus *et al.* (2011)[110]	6 wt% CdS–montmorillonite/ 2.63 ± 0.09 eV	Deposition of originated CdS–CTA micelles on montmorillonite	CO_2 (saturated), NaOH (0.2 mM aqueous solution/8 W Hg lamp (254 nm)/—	(—/—/6.7/24/—), (0.1/—/5 nm particle/ 0.001/suspended)	Methane/0.93/—	• Montmorillonite (MMT) serves as a carrier of CdS nanoparticles that were attached to its external surface • A stirred batch annular reactor is used with a suspended catalyst
X. Li *et al.* (2011)[116]	15% Bi_2S_3–CdS/1.28 eV	Hydrothermal direct reaction	CO_2 (saturated), NaOH–Na_2S aqueous solution (200 mL)/ 500 W Xe lamp (200–700 nm)/—	(—/—/—/5/—), (0.2/24/ 12 nm particles/17/ suspended)	Methanol/120/—	• Results show that the photocatalytic activity and visible light response of Bi_2S_3 are higher than those of CdS • Reaction is carried out in a XPA-II photochemical reactor with a magnetic stirrer, a quartz cool trap, and a condensation tube
Barton *et al.* (2008)[121]	p-GaP/2.24 eV	—	CO_2 (—), pyridine (10 mM)/200 W Hg–Xe arc light (365 nm)/ 0.92 mA cm^{-2}[b]	(—/—/5.2/—/44), (—/—/semiconductor/ electrodes/—/supported)	Methanol/—/10.9	• An aqueous photoelectrochemical cell is used where light energy is the only energy used to carry out the reaction
Zhang *et al.* (2004)[118]	MnS/3.0 eV	Laboratory synthesis	CO_2 (saturated), deoxygenated water (500 mL)/450 W medium-pressure Hg arc lamp (200–400 nm)/0.6 mW cm^{-2}	(308/—/7.5/0.5/4.5), (0.5/—/particles/0.001/ suspended)	Formate/220[d]/—	• Results represent some of the prebiotic syntheses that have arisen *via* photoelectrochemical reactions on semiconducting minerals • Insufficient reductiveness of conduction-band electrons is a limitation in this system • The reaction is carried out in a commercial photochemical reactor consisting of a 0.5 L glass reaction vessel with a water jacket for temperature control

Table 4 (*Contd.*)

Researcher (year) and ref.	Catalyst/band gap energy	Catalyst treatment/preparation technique	Reactants (amount)/ radiation source/ light intensity	Operating conditions (T/P/pH/t/QE), operating variables (W/SA/PS/SC/MP)	Major product/yield (μmol h^{-1} per g catalyst)/ efficiency (%)	Comments
Y. Shioya *et al.* (2003)[127]	Ti-mesoporous silica thin film (hexagonal)/—	Solvent evaporation method	CO_2 (36 μmol), water vapor (180 μmol)/100 W high pressure Hg lamp/0.265 mW cm^{-2}	(323/9.8 × 10^{-10}/—/6/ 0.28), (0.05/900/1.9 nm pore size/—/supported)	Methane, methanol/7.2, 1.98/—	• Advanced transparent Ti-containing thin film is used as photocatalysts having unique and high photocatalytic activity • The films have hexagonal pore structure with higher photocatalytic activity than the Ti-MCM-41 powdered catalyst even with the same pore structure • A quartz cell with a flat bottom (88 cm^3) is used to carry out the reaction
K. Ikeue *et al.* (2002)[128]	Ti-containing porous silica thin films/—	Solvent evaporation method	CO_2 (36 μmol), water vapor (180 μmol)/100 W Hg lamp/0.265 mW cm^{-2}	(323/9.8 × 10^{-10}/—/8/ 0.28), (0.05/—/thin nanofilm/—/supported)	Methane, methanol/8.75, 2.12/—	• Self-standing porous silica thin films with hexagonal pore structures are used as photocatalysts and show higher photocatalytic activity than the same pore-structured Ti-MCM-41 powder catalyst • The concentration of the surface OH groups has a role in the high selectivity • Reaction is conducted on a quartz cell with a flat bottom (88 cm^3) linked to a conventional vacuum system
K. Ikeue *et al.* (2001)[129]	Ti–β-zeolite	Hydrothermal synthesis method	CO_2 (36 μmol), H_2O (180 μmol)/100 W high-pressure Hg lamp (>250 nm)/ 0.265 mW cm^{-2}	(323/9.8 × 10^{-10}/—/6/—), (0.05/630/0.25–0.50 μm particles/—/suspended)	Methane/5.5/11	• Ti–β-zeolite shows the titanium oxide species are highly dispersed in their frameworks in a tetrahedral coordination state • H_2O attraction to the zeolite surface run to a strong influence on the reactivity and selectivity • The properties of the zeolite cavities are important factors to regulate the reactivity and selectivity
Ulagappan and Frei (2000)[130]	Ti silicalite (TS-1) molecular sieve/—	Promoter-induced enhancement method	CO_2(saturated), methanol (—)/266 nm pulsed Nd : YAG laser at 10 Hz/30 mW cm^{-2}	(298/0.0066/—/4/—), (0.022/—/266 nm sieve nanocomposite/—/ supported)	Formic acid, carbon monoxide/—/—	• TS-1 wafer is held in a small infrared vacuum cell with CaF_2 windows, which is fixed inside an Oxford cryostat model Optistat • This study first represents the understanding into the initial steps of CO_2 photoreduction in a framework Ti molecular sieve
Hinogami *et al.* (1998)[125]	Cu, Ag, Au–(p-Si)/ 1.12 eV	Metal particles are deposited on p-Si electrode	CO_2 (saturated), $KHCO_3$ (0.1 M)/ tungsten-halogen lamp/100 mW cm^{-2}	(298/1/6.8/—/—), (—/—/particles on Si electrode/—/supported)	Carbon monoxide, hydrogen/—/—	• Photoelectrochemical reduction is carried out on p-type silicon electrodes modified with small metal (Cu, Ag, or Au) particles • Reaction is conducted on H-shaped Pyrex cell with a reference calomel electrode and a Pt plate as the counter electrode

Table 4 (*Contd.*)

Researcher (year) and ref.	Catalyst/band gap energy	Catalyst treatment/preparation technique	Reactants (amount)/ radiation source/ light intensity	Operating conditions (T/P/pH/t/QE), operating variables (W/SA/PS/SC/MP)	Major product/yield (μmol h^{-1} per g catalyst)/ efficiency (%)	Comments
B. R. Eggins *et al.* (1998)[111]	CdS colloids/2.4 eV	Laboratory synthesis	CO_2 (saturated), TMACl (solution)/ medium pressure Hg lamp/2.5 × 10^{-3} einsteins per h	(—/—/4/42/0.48), (0.3/—/2–4 nm nanoparticle/—/ suspended)	Glyoxylate/53[e]/—	• Photoreduction using ZnO, SiC, $BaTiO_3$ and Sr TiO_3 in absence of tetramethylammonium ions produced formate and formaldehyde • In this system, the effectiveness of hole–acceptor compounds is shown to be related to their redox potentials
B.-J. Liu *et al.* (1998)[112]	CdS surface modified by thiol/—	Laboratory synthesis	CO_2 (—), 2-propanol (1 M)/500 W high pressure Hg arc lamp (300 nm)/1000 mW cm^{-2}	(298/—/—/7/—), (0.72/—/50 nm particle/—/suspended)	Formate, carbon monoxide/1.5, 0.75[f]/—	• It is found that formate to carbon monoxide production became greater with increase of the surface modification of CdS • A quartz cell of a 7.0 cm^3 capacity is used to carry out the reaction with sealed top by a rubber septum
H. Fujiwara *et al.* (1998)[106]	ZnS–DMF(OAc)/—	Colloidal ZnS–DMF is prepared from deaerated DMF solution of $Zn(OAc)_2$	CO_2 (saturated), deaerated DMF solvent (2 mL)/UV light (>290 nm)/—	(298/—/—/5/—), (10^{g}/—/2 nm nanoparticle/—/ suspended)	$HCOO^-$/—/—	• Excess zinc acetate increases the efficiency of the system and prevents the formation of sulfur vacancies as catalytic sites • Together, $HCOO^-$ and CO are produced in the presence of excess zinc perchlorate in this system
H. Fujiwara *et al.* (1997)[113]	CdS surface modified by DMF/ 2.4 eV	Laboratory synthesis	CO_2 (—), TEA (1 M)/ 300 W halogen tungsten lamp (>400 nm)/—	(298/—/—/—/—), (—/—/nanocrystallites/—/ suspended)	Carbon monoxide/—/—	• Addition of excess Cd^{2+} to the system increases the photocatalytic activity • Sulfur vacancies supported by *in situ* Cd changes the coordination numbers of cadmium–sulfur and cadmium–oxygen • A closed Pyrex tube (8 mm diameter) is used to conduct the photoreduction
H. Inoue *et al.* (1995)[117]	0.025 mol% Cd–ZnS/3.66 eV	Photodeposition method	CO_2 (saturated), $NaHCO_3$ (50 μL, 1.5 × 10^{-3} M solution)/ 500 W high-pressure Hg arc lamp/—	(—/—/5.5/1/32.5), (—/200/ nanoparticle/—/ suspended)	Formate/10.5[f]/—	• It is found that solid solutions of ZnS–CdS microcrystals do not show high activities for the photoreduction of CO_2 • The production of CO was observed for a CdS mole fraction of 0.5–0.67
Cook, R. L. *et al.* (1988)[126]	Cu–(p-SiC)/—	Suspensions of p-SiC and Cu particles	CO_2 (—), $KHCO_3$ (0.5 M aqueous solution)/ Hg lamp (>275 nm)/8 mA cm^{-2}	(313/1/—/—/6), (0.1/—/ particles/—/suspended)	Methane/0.63/—	• It is found that formaldehyde can be reduced in an aqueous electrolyte to give methane • Photoelectrochemical (PEC) reduction of CO_2 is done in this system

Table 4 (*Contd.*)

Researcher (year) and ref.	Catalyst/band gap energy	Catalyst treatment/preparation technique	Reactants (amount)/ radiation source/ light intensity	Operating conditions (T/P/pH/t/QE), operating variables (W/SA/PS/SC/MP)	Major product/yield (μmol h^{-1} per g catalyst)/ efficiency (%)	Comments
Aurian-Blajeni *et al.* (1983)[124]	p-GaAs/—	—	CO_2 (saturated), KCl (0.5 M solution)/150 W Xe lamp/—	(298/8.5/—/—/—), (—/—/semiconductor electrode/—/supported)	Formic acid/170[f]/—	• A photoelectrochemical autoclave, fitted with a quartz window is used to carry out the reaction • Adsorption of the CO_2 on the semiconductor surface clearly plays an important role in the process • The electrodes are not stable and have worsened noticeably within several hours
Inoue *et al.* (1979)[42]	CdS, GaP and SiC/ 2.4, 2.3 and 3.0 eV	Purity 99.5 to 99.99%	CO_2 (saturated), H_2O (100 mL)/500 W Xe or high pressure Hg lamp/—	(298/1/5/7/—), (1/—/ 200–400 mesh powder/—/suspended)	Formaldehyde, methanol/ (29, 17), (14, 16) and (14, 76)/—	• Magnetic stirred glass cell with quartz window is used for photoreduction of CO_2 • Photoexcited electrons in the more negative conduction band poses higher ability to reduce CO_2
M. Halmann (1978)[119]	p-GaP single crystal/ 2.25 eV	—	CO_2 (saturated), K_2HPO_4 solution (0.05 M)/high pressure Hg lamp/ 2.63 mW cm^{-2}	(298/—/6.8/90/—), (—/2.4 $\times$ 10^{-5}/ semiconductor electrode/—/supported)	Formic acid/50[g]/0.61	• Closed bubble-walled borosilicate glass beaker (30 mL) with thermostat is used as a photoelectrochemical reactor

[a] T/P/pH/t/QE: temperature (K)/pressure (atm)/pH/illumination period (hours)/quantum efficiency (%). W/SA/PS/SC/MP: weight of photocatalyst (g)/surface area (m^2 g^{-1})/photocatalyst structure (diameter)/semiconductor concentration (g mL^{-1})/mode of photocatalyst. '—': not mentioned in the original paper. [b] Current density. [c] μmol h^{-1}. [d] μM. [e] μmol dm^{-3}. [f] μmol. [g] mM.

effectively in the photoreaction. Zhang *et al.* introduced another metal sulphide semiconductor catalyst (MnS), which can be used under the solar spectrum more competently due to low band gap energy (3.0 eV).[118] Similar to CdS, MnS semiconductor materials also have the distinct behavior of containing high-reducing conduction band electrons which are satisfactorily active for encouraging the reduction of CO_2.[118] That is why, MnS semiconductors deliver higher quantum efficiency than other common catalysts such as TiO_2.

2.2.2 Metal phosphide semiconductor. The use of catalysts for photochemical purposes without incorporating co-catalysts such as p-type GaP and p-type InP have also been studied due to narrow band gaps to facilitate the visible light response.[119,120] Basically, in the photoelectrochemical CO_2 conversion process, p-type metal phosphides (GaP) were used mainly in methanol production but needed remarkably high over-potentials.[121] However, high faradaic efficiencies for the photo-electrochemical reduction of CO_2 to CO have also been investigated, while electrolytes are used in nonaqueous forms. Nevertheless, high over-potential is necessary to obtain high faradaic efficiency.[122] Barton *et al.* found that p-type GaP was able to obtain faradaic efficiency of 100% while converting CO_2 to methanol at low potentials, which was more than 300 mV below the standard potential of −0.5 V *versus* the saturated calomel electrode (SCE).[121] Habisreutinger *et al.* reported that p-type GaP semiconductor exhibits low band gap energy (2.24 eV) and possesses high reducing conduction band electrons to ease the reduction of CO_2.[35] On the other hand, for CO_2 photocatalytic conversions, it was detected that p-type InP provided high selectivity for formic acid in a photo-electrochemical cell.[123] Moreover, according to Kaneco *et al.*, p-InP is an active substantial for the photoelectrochemical reduction of CO_2, which revealed higher positive potential of 0.2–0.4 V than that of p-Si and p-GaAs photocathodes in the electrolysis of methanol electrolyte.[120]

2.2.3 Other non-oxide semiconductors. Aurian-Blajeni *et al.* were carried out in the aqueous CO_2 photo-electrochemical reduction by using p-GaP and p-GaAs as photocathodes.[124] In case of p-GaP, the Faradaic yield decreases when the reaction is carried out at a more negative potential, whereas the opposite behavior is shown in the case of p-GaAs electrode. The different behavior of the two electrodes is probably connected to the greater stability of GaP towards anodic decomposition, while in the case of the unstable GaAs, the higher number of negative potentials provide a degree of cathodic protection. Modified p-type silicon (p-Si) electrodes with Cu, Ag, and Au foreign elements have been investigated by Hinogami *et al.*, and were determined to have extraordinary activation energy for CO_2 photoreduction.[125] Metal element deposition on p-Si electrodes not only induce the photo-catalytic activity but also produce high photovoltages. Moreover, CO_2 photochemical reduction is activated by an upward shift of surface band energies of p-Si in terms of achieving energy levels, which is identical between the semiconductor and solution reactants.[125] In another study, p-type SiC modified by Cu particles was also investigated to determine the photo-electrochemical ability in CO_2 reduction.[126]

Ti containing mesoporous silica thin-film materials have been introduced in the photochemical reduction of CO_2 due to their unique and high photocatalytic performances.[127] Spectroscopic analysis proved that Ti ions were highly dispersed in silica networks, and the silica thin films acted as effective photocatalysts during the photoreactions. Besides, the hexagonal pore construction inside the films revealed superior photosensitivity compared with the same pore-structured Ti-MCM-41 powdered catalyst.[127,128] Moreover, FTIR investigation found that Ti containing silica thin film-possessed surface OH groups in various concentrations had a significant influence on CH_3OH formation.[128] Ikeue *et al.* also studied Ti containing β-zeolite treated with OH^- and F^- ions as structure-directing agents (SDA) showed hydrophilic and hydrophobic properties, respectively.[129] Hydrophilic properties show high photocatalytic efficiency due to the easy interaction of H_2O molecules with the tetrahedrally coordinated titanium oxide species on Ti–β-zeolite (OH) than on Ti–β-zeolite (F).

2.3 Doped photocatalysts

To introduce impurities into an extremely pure semiconductor, doping of foreign elements is deliberately inserted for the purpose of controlling its electrical properties. Due to large band gaps, unmodified semiconductor photocatalysts cannot effectively absorb solar radiation with photon energy 1.7–3.1 eV.[131] To decrease its band gap energy, surface modification of the photocatalysts has been attempted by applying stress along the soft direction of a layered semiconductor,[131] introducing oxygen vacancies in semiconductors,[132] or incorporating foreign elements.[133–139] The schematic photocatalytic view of a doped semiconductor is illuminated in Scheme 1(c). Not only that, the recent advancement in different types of doped metal and non-metal elements incorporated with semiconductors found in various research for the photocatalytic conversion of CO_2 has been reported in Tables 5 and 6, respectively.

2.3.1 Noble metal doped semiconductors. Doping metal on semiconductor acts as an electron trap to provide electrons to CO_2. The photoexcited electrons are shifted from the conduction band of the semiconductor to doped metal to leave the holes on the surface of semiconductor.[37] Noble metals, including Ru, Rh, Pd, Ag, Pt, Cu, Ni and Au, have been commonly used with semiconductors as dopants due to Fermi-level or electron-accepting areas at an energy just beneath the conduction band of semiconductors for the photochemical reduction of CO_2. Among those metals, Pt was widely used in many investigations. For example, the TiO_2 semiconductor was doped with 0.5 wt% Pt by wet impregnation to avoid very low photocatalytic activity.[140,141] More homogeneous dispersion of 0.5 wt% Pt on the TiO_2 surface drives the reaction rate swiftly in the both liquid and gas phases.[142] It is found that Pt loaded on TiO_2 transforms active sites from Ti^{4+} to Ti^{3+} by shifting electrons from TiO_2 to Pt, and this phenomena facilitates visible light response.[143] Another investigation shows that Pt doping on anchored titanium oxide catalysts within the Y-zeolite cavities encourages charge separation and increases the formation of CH_4 *in lieu* of CH_3OH by promoting the reaction between the

Table 5 Advances in catalysts that are modified by metal doping for CO_2 photoreduction[a]

Researcher (year)/ref.	Catalyst composition/ band gap energy	Catalyst preparation/ treatment technique	Reactants (amount)/ radiation source/ light intensity	Operating variables (T/P/pH/t/QE), physical properties (W/SA/PS/SC/MP)	Major product/Yield (μmol h^{-1} per g catalyst)/selectivity (%)	Comments
Q. Zhai *et al.* (2013)[167]	1.7 wt% Cu–0.9 wt% Pt–TiO_2/—	Photodeposition technique	CO_2 (saturated), H_2O (4.0 mL)/200 W Xe lamp (320–780 nm)/—	(323/2/—/4/—), (0.02/—/7.3 nm particles/—/ suspended)	Methane/33/85	• Cu_2O delivers sites for the activation of CO_2 in presence of H_2O, while Pt extracts the photogenerated electrons from TiO_2 • A stainless-steel reactor with a quartz window on the top is used to carry out the reaction
B. D. Mankidy *et al.* (2013)[169]	Ag–Pt–TiO_2/—	Galvanic replacement reaction and sol–gel method	CO_2 (—), water vapor (—)/100 W Hg lamp (330 nm)/—	(298/1/—/6/—), (1/—/nanoparticles/ —/supported)	Methane/—/80	• Combination of both bimetallic co-catalysts and Ag–SiO_2 nanoparticles increase product yields and enhanced activity in comparison to native TiO_2 • A batch reactor is used with three optical windows; one glass window at the top for photoirradiation and two ZnSe windows on two sides
P. Li *et al.* (2012)[145]	0.5 wt% Pt–$NaNbO_3$/ 3.29 eV	Typical furfural alcohol derived polymerization – oxidation process	CO_2 (saturated), H_2O (3 mL)/300 W Xe arc lamp/—	(—/0.78/—/8/—), (0.1/28.6/powder/—/ supported)	Methane/4.9/—	• It is found that H_2 development and CO_2 reduction over cubic $NaNbO_3$ are nearly twice of those over orthorhombic $NaNbO_3$ • Cubic $NaNbO_3$ can be qualified to its unique electronic structure, which is useful for electron excitation and transfer • Catalysts are put on a small glass cell inside the Pyrex reaction cell with gas closed circulation system
H. Shi and Z. Zou (2012)[144]	Pt–$KNbO_3$/3.1 eV	Solid state reaction	CO_2 (saturated), H_2O (3 mL)/300 W Xe lamp/—	(—/—/—/6/—), (0.1/ 3.4/1 μm particle/—/ suspended)	Methane/70[b]/—	• It is detected that $KNbO_3$ displays a higher photocatalytic activity than $NaNbO_3$ due to the narrower band gap and higher mobile charge carriers • Catalysts are uniformly put on the bottom of a small glass cell that is placed in a Pyrex glass cell
K. Iizuka *et al.* (2011)[154]	1 wt% Ag–$BaLa_4Ti_4O_{15}$, and Ag–$SrLa_4Ti_4O_{15}$/3.79 and 3.8 eV	Polymerizable complex method and impregnation method	CO_2 (saturated), H_2O (360 mL)/400 W high pressure Hg lamp/—	(—/—/—/7/—), (0.3/—/10 nm particles/—/ suspended)	Carbon monoxide, formic acid/(17.33, —) and (7.7, 4.3)/—	• Ag co-catalyst performs as a CO_2 reduction site to form CO • Development of O_2 in a stoichiometric ratio (H_2 + CO : O_2 = 2 : 1 in a molar ratio) shows that water is used up as a reducing reagent • An inner irradiation cell made of quartz is used to carry out the photocatalytic reduction of CO_2

Table 5 (*Contd.*)

Researcher (year)/ref.	Catalyst composition/ band gap energy	Catalyst preparation/ treatment technique	Reactants (amount)/ radiation source/ light intensity	Operating variables (T/P/pH/t/QE), physical properties (W/SA/PS/SC/MP)	Major product/Yield (μmol h^{-1} per g catalyst)/selectivity (%)	Comments
C.-C. Yang *et al.* (2011)[162]	0.05 wt% Ti-SBA-15/—	Synthesized by filtration, washing, drying, and calcination at 550 °C for 6 hours	CO_2 (saturated), water vapor (76 μmol)/120 W high pressure Hg lamp (280 nm)/150 mW cm^{-2}	(313/1/—/7/—), (0.05/81/nano-porous, 3.2 nm pore size/—/supported)	Ethane, methane/0.02, 0.016/—	• A combination of CO and H_2O leads the highest amounts of CH_4, C_2H_4, and C_2H_6, whereas a mixture of CO_2 and H_2 leads the lowest production rate of these products • A multiple batch cylindrical photoreactor (50 mL) is used to conduct the reaction
T. Yui *et al.* (2011)[52]	2 wt% Pd–TiO_2/—	Photochemical deposition	CO_2 (saturated), H_2O (1.5 mL)/500 W high-pressure Hg arc lamp (>310 nm)/—	(278/—/4.1/5/—), (0.15/—/ nanoparticle/0.1/ suspended)	Methane/0.56/—	• Lengthy irradiation shows deactivation of the photocatalysis of Pd–TiO_2 due to the partial oxidation of the deposited Pd to PdO • Catalysts are put in a round-shaped quartz vessel with an inner diameter of 6 cm
N. Zhang *et al.* (2011)[146]	1 wt% Pt–Zn_2GeO_4/4.5 eV	Ion exchange method	CO_2 (saturated), H_2O (—)/Arc Xe lamp (635 nm)/—	(298/—/14/12/0.2), (—/90.5/200 nm particle/—/ supported)	Methane/28.9[b]/—	• Ion exchange synthesized catalyst shows activity in photoreduction of CO_2, compared with Zn_2GeO_4 synthesized by a solid–state reaction
C. Wang *et al.* (2011)[170]	[ReI(CO)$_3$(dcbpy)Cl]-$Zr_6O_4(OH)_4$(bpdc)/—	Mix-and-match synthetic strategy	CO_2 (—), Acetonitrile (2 mL) and TEA (0.1 mL)/ 450 W Xe lamp (>300 nm)/—	(—/—/—/16/—), (0.02/277/metal–organic frameworks/—/ suspended)	Carbon monoxide/42/—	• These stable and porous metal complex-derivatives-doped metal organic frameworks are very active catalysts for a range of reactions related to solar energy application
C. Ampelli *et al.* (2010)[142]	0.5 wt% Pt–TiO_2/—	Sol–gel dipcoating for TiO_2 film and wet impregnation to add Pt	CO_2 (—), NaOH (1 M aqueous solution)/ 60 W solar lamp/—	(313/19.3/—/7/—), (—/—/nanoparticle/ —/supported)	Hydrogen/5.3[c]/—	• Require development of the current limits, related to the design of the photoanode and electrocathode to increase activity • Photoelectrochemical solar cell is designed by Plexiglas and equipped with a quartz window and 5.7 cm^2 irradiated area
A. Nishimura *et al.* (2010)[159]	Cr–TiO_2/—	Sol–gel and dip-coating method	CO_2 (5.76 mmol), H_2O (5.56 mmol)/Xe arc lamp (185–2000 nm)/43.67 mW cm^{-2}	(343/9.8/—/72/—), (—/—/film/3.9/ supported)	Carbon monoxide/ 1285/—	• The total layer number of Cr-doped TiO_2 film coated is up to 7 • Cr–TiO_2 film is inserted into the stainless pipe, equipped with quartz glass disc fixed to the top of the stainless pipe
Nguyen and Wu (2008)[165]	1 wt% Cu–Fe–TiO_2 films/2.93 eV	Dip-coating method or doctor blade technique	CO_2 (saturated), water vapor (—)/150 W UVA lamp (320–500 nm)/225 mW cm^{-2}	(348/—/5/4/0.001), (—/47.74/film of 878 nm thickness/—/ supported)	Methane, ethylene/0.06, 0.35/—	• A continuous circular Pyrex glass reactor (216 cm^3) with a quartz window, where catalyst coated optical fibers are gathered inside it • Fe as a co-dopant is indicated to reduce the photoproduction of methane in this experiment

Table 5 (*Contd.*)

Researcher (year)/ref.	Catalyst composition/ band gap energy	Catalyst preparation/ treatment technique	Reactants (amount)/ radiation source/ light intensity	Operating variables (T/P/pH/t/QE), physical properties (W/SA/PS/SC/MP)	Major product/Yield (μmol h^{-1} per g catalyst)/selectivity (%)	Comments
Nguyen and Wu (2008)[166]	0.5 wt% Cu–Fe–(TiO_2–SiO_2)/2.95 eV	Sol–gel method	CO_2 (saturated), H_2O (—)/natural sunlight/2.05 mW cm^{-2}	(348/—/—/6/0.0182), (0.5/44.7/53 nm thickness film/—/ supported)	Methane/0.279/0.0152	• Introducing Fe metal into TiO_2–SiO_2 lattice shows the full visible light absorption and superior production of methane, compared with that of the bare TiO_2–SiO_2–acac • A continuous circular Pyrex glass reactor (216 cm^3) with a quartz window, where the catalyst coated optical fibers are gathered inside it
J.-S. Hwang *et al.* (2005)[163]	0.29 wt% Ti-SBA-15 (Si/Ti = 270)/—	Modified hydrothermal method	CO_2 (36 μmol), water vapor (180 μmol)/ 100 W high pressure Hg lamp (>250 nm)/—	(323/9.8 × 10^{-10}/—/ 12/—), (0.05/1040/ 6.9 nm pore size/—/ immobilized)	Methane, methanol/ 0.31, 0.081/—	• Ti-SBA-15 shows reactivity much higher than bulk TiO_2 • Cationic rhenium(I) complex into a mesoporous AlMCM-41 material by ion-exchange method shows visible light response • A quartz cell (88 cm^3) with a flat bottom is used to carry out the reaction
G. Guan *et al.* (2003)[158]	Pt–$K_2Ti_6O_{13}$ with Fe-based catalyst supported on Y-type zeolite/—	Steam dealumination, impregnation and photochemical deposition method	CO_2 (saturated), H_2O (4 mL)/300 W Xe lamp, or concentrated sunlight/—	(298/0.76/—/6/—), (0.3/—/powder/—/ supported)	Hydrogen/15.2/—	• The reaction temperature expressively influenced by concentrating the solar irradiation, reaching 600 K and increasing the yields • Catalysts are kept on wet quartz wool (a wet bed for the catalyst layer) in an optical quartz tube cell
I.-H. Tseng *et al.* (2002)[150]	2 wt% Cu–TiO_2/—	Modified sol–gel process	CO_2 (—), NaOH (300 mL, 0.2 N aqueous solution)/Hg lamp (254 nm)/—	(323/—/7/6/—), (0.3/ 26/20 nm particle/—/ suspended)	Methanol/20/—	• Result shows that a higher positive zeta potential at pH 7 can lead higher activity • A cylindrical quartz reactor with a capacity of 300 mL is used to carry out the reaction
M. Anpo *et al.* (1998)[171]	1.0 wt% Pt-Ti-MCM-48 (Si/Ti = 80)/—	Hydrothermal and impregnation methods	CO_2 (24 μmol), water vapor (120 μmol)/ high pressure Hg lamp (>280 nm)/—	(328/1.3 × 10^{-9}/—/—/—), (—/—/>2 nm pore size/—/supported)	Methane/12/—	• The charge transfer excited state of highly dispersed titanium oxide species plays an important role in the reduction of CO_2 and shows a high selectivity for the formation of CH_3OH • A quartz cell with a flat bottom is used to reduce CO_2 with H_2O
M. Anpo *et al.* (1997)[82]	1 wt% Pt–(TiO_2–Y-zeolite)/—	Impregnation method	CO_2 (24 μmol), water vapor (120 μmol)/75 W high-pressure Hg lamp (>280 nm)/—	(328/1.3 × 10^{-9}/—/ 6/—), (0.15/—/ powder/—/ supported)	Methane/0.08/—	• The titanium oxide species are highly dispersed within the zeolite cavities and exist in a tetrahedral coordination • Adding Pt to the anchored titanium oxide catalysts encourages the charge separation with increasing CH_4 yields in place of CH_3OH

Table 5 (*Contd.*)

Researcher (year)/ref.	Catalyst composition/ band gap energy	Catalyst preparation/ treatment technique	Reactants (amount)/ radiation source/ light intensity	Operating variables (T/P/pH/t/QE), physical properties (W/SA/PS/SC/MP)	Major product/Yield (μmol h^{-1} per g catalyst)/selectivity (%)	Comments
Solymosi and Tombacz (1994)[73]	1 wt% Rh–TiO_2/—	Wet impregnation method	CO_2 (saturated), H_2O (120 mL)/500 W high pressure Xe lamp/0.68 mW cm^{-2}	(333/1/—/5/—), (0.3/ 18/nanoparticle/ 0.0025/suspended)	Formic acid/1.6/—	• An increase in the electron concentration of TiO_2 enhances the production of organic compounds • A Pyrex glass cell is used to carry out the photocatalytic reduction of CO_2 with H_2O
K. Adachi *et al.* (1994)[151]	5 wt% Cu–TiO_2/—	Impregnation method	CO_2 (27.09 atm), H_2O (30 mL)/450W Xe lamp/—	(298/1/5.45/48/—), (0.5/8.7/230 nm particle/—/ suspended)	Methane/0.02/—	• Low yield and compulsory separation of the gaseous products may create drawbacks for this system • Catalysts are placed in a stainless-steel vessel (42.5 mL) with a quartz window to run the photocatalytic reduction of CO_2
J. C. Hemminger *et al.* (1978)[172]	$SrTiO_3$–Pt/3.2 eV	—	CO_2 (0.019 atm), water vapor (0.022 atm)/500 W high pressure mercury lamp/—	(315/1/—/0.5/0.01), (—/—/particle/—/ supported)	Methane/—/—	• A batch type isolation chamber is used to carry out the reaction and the samples are kept on a small disk of 1 cm^2 area • The photo and thermal processes are easily distinguished by the filters used in this experiment

[a] T/P/pH/t/QE: temperature (K)/pressure (atm)/pH/illumination period (hours)/quantum efficiency (%). W/SA/PS/SC/MP: weight of photocatalyst (g)/surface area (m^2 g^{-1})/photocatalyst structure (diameter)/semiconductor concentration (g mL^{-1})/mode of photocatalyst. '—': not mentioned in the original paper. [b] ppm h^{-1} g^{-1} catalyst. [c] mmol h^{-1} g^{-1} catalyst.

Table 6 Advances in non-metal-doped and modified catalysts for CO_2 photoreduction[a]

Researcher (year) and ref.	Catalyst composition/ band gap energy	Catalyst preparation technique	Reactants (amount)/ radiation source/ light intensity	Operating variables (T/P/pH/t/QE), physical properties (W/SA/PS/SC/MP)	Major product/yield (μmol h^{-1} per g catalyst)/selectivity (%)	Comments
Q. Zhang *et al.* (2011)[190]	10 wt% I doped TiO_2 at 375 °C/3.0 eV	Hydrothermal method	CO_2 (saturated), water vapor (0.022 atm)/450 W Xe lamp (>400 nm)/233 mW cm^{-2}	(—/—/—/3.5/—), (0.2/137.6/<45 μm nanoparticle/—/ supported)	Carbon monoxide/ 2.4/—	• Samples are put on a glass-fiber filter at the bottom of the cylindrical photoreactor (58 cm^3) with stainless steel walls and a quartz window • High CO_2 reduction activity is detected for I–TiO_2 under visible light than undoped TiO_2 under UV-vis irradiation • Too high an iodine-doping level may create recombination centers and thus lower the photocatalytic activity
T. M. Suzuki *et al.* (2011)[182]	N–Ta_2O_5 anchored with Ru-dpbpy/2.4 eV	Direct assembly method	CO_2 (saturated), MeCN : TEOA (5 : 1, 4 mL solution)/500 W Xe lamp (410–750 nm)/—	(—/—/—/60/—), (0.01/—/20–40 nm nanoparticle/—/ suspended)	Formic acid/60[b]/—	• It is found that the photocatalytic activity and stability of the hybrid catalyst depends on the chemical structure of the anchor group
C.-W. Tsai *et al.* (2011)[184]	0.42 wt% N doped $InTaO_4$ with 3.2 wt% Ni–NiO core shell/2.28 eV	Impregnation method	CO_2 (saturated), deionized water (50 mL)/Xe lamp/—	(298/—/—/2/—), (0.1/—/40 nm particles/—/ suspended)	Methanol/165/—	• Nitrogen doping shows visible light responsive photocatalytic activity with additionally high absorbance and gives approximately twice the yield of undoped ones, while the co-catalytic method gives about triple the yield • Reaction is conducted on a stirred-type, continuous-flow reactor having a window-type irradiation cell that is made of Pyrex glass (200 mL)
L.-M. Xue *et al.* (2011)[185]	C doped TiO_2/—	Immersion and calcination methods	CO_2 (saturated), H_2O (10 mL)/175 W high pressure Hg lamp/—	(—/—/2/6/—), (1/—/ nanopowder/—/ suspended)	Formic acid/439/—	• The doped carbon shows low-band gap and expends the absorption of visible light region under the simulated daylight lamp • A three-concentric cylindrical quartz reactor is used having outermost layer for reaction pool, the middle layer for quartz cold trap and the innermost layer as the light source
S. Sato *et al.* (2010)[183]	N–Ta_2O_5 linked with Ru-dcbpy/2.4 eV	Thermal treatment method	CO_2 (saturated), MeCN : TEOA (5 : 1, 4 mL solution)/Xe lamp (405 nm)/—	(298/—/—/20/1.9), (0.005/—/ nanoparticles/—/ suspended)	Formic acid/70/75	• Visible light is used to irradiate 8 mL test tubes containing the photocatalysts • The linkage between the complex and the semiconductor greatly increases the reaction rate
O. K. Varghese *et al.* (2009)[168]	Nitrogen-doped titania nanotube with copper/—	Anodization and annealed at 460 or 600 °C for 3 h	CO_2 (saturated), water vapor (saturated)/ sunlight/100 mW cm^{-2}	(317/<0.068/—/3.5/—), (—/—/nanoparticle/ —/supported)	Methane/4.4/—	• CO_2 to hydrocarbon production rate under outdoor solar light is at least 20 times higher than using UV illumination • Samples are loaded into a stainless-steel chamber having an O-ring sealed quartz window at the top for admitting solar radiation • Identical construction of two chambers having volumes 7.5 cm^3 and 8.6 cm^3 are used to allow for two samples simultaneously

[a] T/P/pH/t/QE: temperature (K)/pressure (atm)/pH/illumination period (hours)/quantum efficiency (%). W/SA/PS/SC/MP: weight of photocatalyst (g)/surface area (m^2 g^{-1})/photocatalyst structure (diameter)/semiconductor concentration (g mL^{-1})/mode of photocatalyst. '—': not mentioned in the original paper. [b] Turn over number.

arbon radicals and H atoms formed on the Pt metals.[82] Pt-loaded alkali niobates $ANbO_3$ (A = Na, K) photocatalysts were reported by Li *et al.*[144] Results showed that $KNbO_3$ exhibited higher photocatalytic activity than $NaNbO_3$ because of having low band gap energy (E_g) and high mobile charge carriers. Here, Pt acts as a co-catalyst to provide the reactive site for hydrogen gas production easily in terms of low H_2 over-potential on the Pt surface.[145] It is also noticeable that increasing Pt proportion from 0.5 wt% to 1.0 wt% promotes the formation of hydrogen gas. The photocatalytic performance of micro- or mesoporous Zn_2GeO_4 loading with various percentages of Pt (from 0.5 to 2.5 wt%) was investigated by N. Zhang *et al.*, from which the results evaluated the highest activity for 1.0 wt% Pt.[146]

Ishitani *et al.* reported that Pd doped on TiO_2 performed more effective photocatalytic activity than that of other metals loaded on TiO_2, and it also increased the formation of CH_4 instead of CO from CO_2.[147] On the other hand, Pd on the surface of TiO_2 partially oxidized to form PdO during the progression of CH_4 formation, which led to the deactivation of the Pd–TiO_2 catalysts.[52] Solymosi and Tombacz assumed that adsorption and photocatalytic behaviors of Rh were significantly influenced by the existence of an electronic interaction at the Rh–TiO_2 interface.[73] Moreover, the catalytic activity of Rh was affected by doping with altervalent cations (W^{6+}) due to the variation of the electron concentration of the TiO_2.[148] Cu is another noble metal, which is eminent for its availability and low cost. Not only that, Cu loading on TiO_2 was a prevalent approach in photocatalytic conversion of CO_2 because of its high yield through the lowering of re-electron–hole recombination probability. According to Tseng *et al.*, an optimal Cu-loaded titania (2 wt% Cu) was found to have the highest photochemical activity, which provided lower fluorescence intensity and resulted in higher methanol formation.[149,150] Depending on the amount of Cu loading on TiO_2, the formation of the hydrocarbon products has been changed also.[151] Ag-doped TiO_2 was also investigated in this technology reduced the band gap energy of TiO_2 and shifted the band edge from the UV region to the visible region, according to the amount of Ag added.[152,153] Ag co-catalyst-loaded on $ALa_4Ti_4O_{15}$ (A = Ca, Sr, and Ba) has been published, and Ag acts as a CO_2 reduction site to generate CO as reported in electrochemical reduction of CO_2, where Ag was used as an electrocatalyst.[154] Moreover, the plasmon effect has been developed by Au nanoparticles doped with TiO_2 through increasing the visible light response.[155–157]

2.3.2 Transition metal doped semiconductors. To improve the photocatalytic activity and efficiency, transition metals are also investigated in many studies due to the high visible light conversion of CO_2.[158] The interesting thing about transition metals is that their valence electrons to exhibit several common oxidation states. Among the transition metals, Co, Mn, Ni, Cr, Mo, Fe, V, and Ti are commonly used as doping elements in photocatalytic technology to enhance the semiconductor performances under visible light. For visible light responsibility, Nishimura *et al.* synthesized Cr-doped TiO_2 film by the sol–gel and dip-coating methods.[159] They stated that a suitable percentage of metal doping on semiconductors improved catalytic activity, whereas excess percentages of dopant metal beyond the optimal level decreased the photocatalytic performances because of charge recombination. However, the H_2 generation rate was more advanced for Fe-doped TiO_2 than Cr-doped TiO_2 because of avoiding the recombination in trapping both electrons and holes by Fe particles, whereas Cr can only trap one type of charge carrier.[160] The experiment was done to characterize the different types of transition metals (V, Fe, Ce, Cu, Cr) doped TiO_2, prepared by Pan *et al.*[161] They reported that V and Fe were placed in the substitutional sites of TiO_2, and Ce ions were dispersed in the interstitial sites, although Cr and Cu accumulated on the surface. The activity order was found in such a manner: Fe–TiO_2 > V–TiO_2 > Cr–TiO_2 > Ce–TiO_2 > TiO_2 > Cu–TiO_2, which indicates that the local structure and type of dopant have vital contributions on photocatalytic technology.

The loading of transitional metal species on the framework nanostructure is a common practice for increasing the high dispersion of those species. Moreover, for surface immobilization, titanium species are confined onto mesoporous silica. This phenomenon is also effective for photocatalytic reactions of titanium particles as their photocatalytic activities intensely rely on the structures of active sites.[162] It was found that high and exceptional photocatalytic reactivity was obtained for the reduction of CO_2 with H_2O to generate CH_4 and CH_3OH under UV irradiation, compared with the bulk TiO_2.[163]

2.3.3 Co-metal doped semiconductors. The doping of bimetallic elements together on semiconductor photocatalysts has been validated as a potential method to advance the visible light response of photocatalysts. Suitable co-dopant combinations are necessary to enhance the photocatalytic activity of semiconductors because all of the co-dopant configurations are not appropriate for this technique.[164] Fe as a co-dopant in the Cu–TiO_2 catalyst has been investigated for photocatalytic reduction of CO_2 with H_2O to ethylene at a quantum yield of 0.024%.[165] An efficient charge transfer mechanism occurred in this combination between TiO_2 and Cu as well as Fe as co-dopants. However, Cu co-doped with Fe–TiO_2 on SiO_2 support has also been examined under concentrated natural sunlight with high quantum yield (0.05%) and full absorption of visible light and compared to only Cu co-doped on the Fe–TiO_2 counterpart.[166] The photocatalytic performance of the Cu doped on Pt–TiO_2 catalysts is influenced by the content of Cu loading. The high percentage of Cu loading expressively decreases the formation of H_2 and improves the formation of CH_4 and CO.[167] Varghese *et al.* reported that Pt may have an effect on H_2O activation, whereas Cu plays an important role in activating CO_2 to CO.[168] Bimetallic Ag–Pt were used with the TiO_2 semiconductor catalyst as reported by Mankidy *et al.* who obtained a selectivity of CH_4 of almost 80%, compared with TiO_2 of 20% selectivity.[169] Their investigation found that Ag species had a strong surface plasmon absorption band in the UV-vis region, while the Pt species did not show that behavior. However, the combination of bimetallic Ag–Pt has the ability to tune the electronic properties during photochemical reactions. Not only that, combined Ag–Pt can accumulate the electrons by Ag and transfer the interfacial electron charge from Pt.

2.3.4 Non-metal doped semiconductors. It has been broadly confirmed that doping or co-doping of semiconductor photocatalysts with non-metals such as C, N, S, B and F has shown considerably low band gap energy, compared with metal doping in different experiments, prominent to efficient photocatalytic activity during visible light irradiation.[173–180] In Table 6, the update of major findings and detailed information regarding non-metal-doped semiconductors is given elaborately to evaluate their progress in the photocatalytic conversion of CO_2. Compared with other non-metals, nitrogen-doped semiconductors show the most active results due to the narrow band gap.[181] A high rate of solar conversion of carbon dioxide in the presence of water vapor to methane and other hydrocarbons is attained from nitrogen-deposited titania nanotube arrangements, as reported by Varghese *et al.*[168] Particularly, low wall thickness of nanotube arrays promotes the transfer of efficient carriers to the adsorbing species. From the experiment, it was also found that the incorporation of Pt and Cu nanoparticles on the external surfaces of nanotube arrangements further increases the hydrocarbon yield under the outdoor global AM 1.5 sunlight with 100 mW cm^{-2} intensity. Both Suzuki *et al.* and Sato *et al.* studied p-type, photoactive, nitrogen-doped Ta_2O_5 linkage with metal-complex electrocatalysts, which revealed outstanding photochemical conversion of CO_2 to formic acid under visible light irradiation by increasing the photoexcited electron transfer from the conduction band of the semiconductor to the metal complex.[182,183] The co-catalytic (N-doped $InTaO_4$ modified with Ni–NiO core–shell nanostructure) approach by Tsai *et al.* not only intensely increases solar light absorbance but also competently reduces the electron–hole recombination.[184] The investigation with carbon-doped TiO_2 was done by Xue *et al.* because doped carbon narrows the band gap, shifts the absorption to the visible light region and facilitates the charge separation efficiency.[185] Hiroshi *et al.* reported that the hydrophilic behavior of C-doped TiO_2 semiconductor exhibited visible light response, which was initiated from the localized C (2p) formed above the valence band.[186] S-doped TiO_2 has the ability to reduce the band gap energy and inhibits the alteration of anatase phase into rutile phase at elevated temperatures.[187] Correspondingly, the doping of F on a semiconductor catalyst performs better by decreasing the band gap energy.[188]

Results showed that iodine doping on semiconductor catalysts exhibited higher photochemical activity due to the closer ionic radii of I^{5+} and Ti^{4+} for substituting lattice titanium than other non-metal-doped elements like nitrogen, carbon, boron, and sulfur.[189] Moreover, the replacement of Ti^{4+} with I^{5+} begins charge inequality to the formation of Ti^{3+} surface states that is able to arrest the photoinduced electrons and prevent charge recombination in the photocatalytic conversion of CO_2.[190] Zhang *et al.* found that iodine-doped TiO_2 semiconductors calcined at 375 °C reduced particle sizes significantly and increased photochemical activity.[190] It was also observed that 10% iodine deposition on TiO_2 harvested maximum yield under visible light irradiation compared with the 5% iodine doping on TiO_2.

2.4 Sensitized photocatalysts

For photocatalytic CO_2 conversion, photosensitization of the catalyst is a promising technique which makes the catalyst more sensitive during light irradiation. This practice is generally conducted in photochemical applications under the light sources that have particular wavelength deficiencies for photoexcitation. The mechanism generates photoexcited electrons in the conduction band of photosensitizers under the light source of particular wavelengths, and the electrons are directly shifted to the conduction band of catalysts to make them photoactive under visible light irradiation.[191] According to Tahir and Amin, photosensitization exclusively depends on the suitable sensitizer band gap that could absorb visible light irradiations, and the sensitizer conductance band needed to be higher (more negative) than the catalyst's conductance band to transfer electrons towards the catalyst.[181] Some informative characteristics are represented in Table 7 for different types of sensitized photocatalysts, which are applied in many studies for increasing photocatalytic activity in order to obtain high photon efficiency and selectivity.

2.4.1 Dye sensitized photocatalysts. Dye sensitized photocatalysts are widely used in photochemical technology because of their ability to create photoactive electrons easily by visible light hitting the dye compound. This phenomenon helps to transfer those photoactive electrons from the dye to the catalysts' conduction band for activation during the visible light irradiation.[37] An effective response to visible light and efficient electron transfer can enhance fuel yields. The charge separation can be effectively achieved by adding a co-catalyst to trap the electrons, which is depicted in Scheme 1(d).

Li *et al.* reported that charging of Pt and RuO_2 on dye sensitized hexagonal nanoplates to form micro-octahedron Zn_2SnO_4 enabled the accumulation of photoexcited electrons and holes, respectively.[192] Dye sensitized, Pt loaded, nanosized {010} dominant anatase TiO_2 rods were used to obtain exceptional surface atomic structure for optimum adsorption of dye molecules and encourage electron transmission from excited dye molecules to anatase TiO_2.[193] These occurrences also upgraded the current density and solar energy conversion efficiency of that system. Another investigation found that Ru^{II}(2,2′-bipyridyl-4,4′-dicarboxylate)$_2$-$(NCS)_2$ (basically known as N3-dye) sensitized Cu–Fe loading on the P25 photocatalyst was able to absorb the wavelength of 400–800 nm from solar irradiation.[194] Moreover, the results show that N3-dye is not suitable under artificial light (wavelength range is 320–500 nm) irradiation because before the irradiation, it is dispersed on the matrices of the photocatalysts; as a result, the dye does not show its full response to the light source but using concentrated natural sunlight N3-dye remarkably increases methane yield up to over 100%. Similar results were found by Wu and Chiou in that N3-dye gave effectual charge transfer with higher photoreduction under concentrated sunlight.[195] Moreover, it was also found that N3-dye showed its stability for up to 6 h under both artificial light and concentrated sunlight. Ozcan *et al.* used perylene diimide dyes, which have revealed similar visible light response to the Ru^{II}(2,2′-bipyridyl)chloride hexahydrate.[196] In

Table 7 Advances in sensitized catalyst for CO_2 photoreduction[a]

Researcher (year) and ref.	Catalyst composition/ band gap energy	Catalyst preparation technique	Reactants (amount)/ radiation source/ light intensity	Operating variables (T/P/pH/t/QE), physical properties (W/SA/PS/SC/MP)	Major product/Yield (μmol h^{-1} per g catalyst)/efficiency (%)	Comments
Z. Li *et al.* (2012)[192]	Dye-sensitized Zn_2SnO_4 with 1 wt% Pt and 1 wt% RuO_2/ 3.87 eV	Nucleation processes and solid-state reaction	CO_2 (saturated), water vapor (0.4 mL)/300 W Xe arc lamp/100 mW cm^{-2}	(—/—/—/10/—), (0.1/ 7.71/nanoplates/—/ supported)	Methane/86.7[b]/3.1	• Catalysts are evenly kept at the bottom of a Pyrex glass cell, and the reaction is carried out in a gas-tight condition • The unitary geometry of the photoanode improves the solar energy conversion
J. Pan *et al.* (2011)[193]	Dye-sensitized TiO_2 (anatase) with 1 wt% Pt/3.27 eV	Hydrothermal treatment	CO_2 (saturated), water vapor (—)/solar light/—	(—/—/7/10/7.73), (—/25/nano-sized rods/—/supported)	Methane/2.5/—	• Due to distinctive surface atomic or electronic structure, the nanosized rods show a higher activity in converting CO_2 into CH_4 and a comparable energy conversion efficiency
W.-N. Wang *et al.* (2011)[212]	Sensitized TiO_2–SiO_2 composite with 0.01 mol% Cu/1.2 eV	FuAR method	CO_2 (saturated), deionized water (3.0 g)/Xe arc lamp (250–400 nm)/2.4 mW cm^{-2}	(—/—/—/8/—), (0.02/ 81.71/265 nm composite particles/—/ supported)	Carbon monoxide/20/—	• Size, composition and porosity of the composite particles are tailored by controlling the precursor concentration, stoichiometric ratio and temperature, respectively • The reactor is cylindrically built with a stainless-steel wall and a quartz window 60 mm in diameter and 25 mm deep, vertically facing the solar lighter
W. Hou *et al.* (2011)[211]	Sensitized TiO_2 films with Au/2.5 eV	Sol–gel process	CO_2 (saturated), water vapor (—)/UV lamp (254 nm)/20 mW cm^{-2}	(348/—/—/15/2.3 × 10^{-2}), (—/—/400 nm thickness film/—/ supported)	Methane/22.4[c]/—	• Surface plasmons of the Au nanoparticles create intense electromagnetic fields to enhance sub-band gap absorption in the TiO_2, and improve the photocatalytic activity in the visible range • Reaction is conducted on a sealed 51.6 mL stainless steel reactor with a quartz window, where the photocatalytic films are kept on the catalyst holder, which is on the bottom of the reactor
D. Luo *et al.* (2011)[213]	Sensitized TiO_2 particles with 2 wt% Cu–Ce/—	Wetness impregnation method	CO_2 (saturated), NaOH (0.2 M, 150 mL solution)/125 W UV lamp (365 nm)/—	(343/—/—/16/—), (0.15/ 2.963/powder/—/ suspended)	Methanol/11.3/—	• It is found that Ce atoms affect the reaction more profoundly than Cu atoms do, and Ce atoms activate H_2O and CO_2 molecules • Reaction is carried out in a hermetic high-pressure reaction still equipped with heating and magnetic stirring system
T. W. Woolerton *et al.* (2011)[209]	Enzyme CODHI-modified TiO_2 with ruthenium bipyridyl/—	Standard system protocol	CO_2 (98%), CH_4 (2%)/250 W (24 V) tungsten-halogen bulb (420 nm)/45 mW cm^{-2}	(293/—/6/4/0.07), (0.005/50/nanoparticles (<100 nm)/—/ suspended)	Carbon monoxide/ 255/—	• Reaction is carried out in a pressure vessel containing the suspension was sealed tightly with a rubber septum • Modified enzyme is efficient for CO_2 conversion and sensitized to visible light

Table 7 (*Contd.*)

Researcher (year) and ref.	Catalyst composition/ band gap energy	Catalyst preparation technique	Reactants (amount)/ radiation source/ light intensity	Operating variables (T/P/pH/t/QE), physical properties (W/SA/PS/SC/MP)	Major product/Yield (μmol h^{-1} per g catalyst)/efficiency (%)	Comments
Y. Li *et al.* (2010)[77]	Sensitized TiO_2 with 0.5 wt% Cu on SiO_2/ 3.1 eV	One-pot sol–gel method	CO_2 (saturated), water vapor (—)/Xe lamp (250–400 nm)/ 2.4 mW cm^{-2}	(273/1/7/4/1.41), (0.1/ 386.2/<100 μm powder/—/supported)	Carbon monoxide/45/—	• High surface area mesoporous silica substrate highly improves photoreduction due to better TiO_2 dispersion and increased adsorption of CO_2 and H_2O on the catalyst, and addition of Cu species increases multi-electron reactions • A cylindrical continuous-flow reactor is used with a stainless steel wall and a quartz window with a 6.0 cm diameter and a 2.5 cm depth
K. Kocí *et al.* (2010)[152]	Sensitized TiO_2 particles with 7 wt% Ag doping/2.74 eV	Sol–gel process	CO_2 (saturated), H_2O (100 mL)/8 W Hg lamp (254 nm)/—	(—/—/—/24/—), (—/79.7/1.65 nm particles/0.001/ suspended)	Methane/0.36/—	• Ag impurity inside the TiO_2 shifts the absorption edge to visible light and forms Schottky barrier at the metal–semiconductor interface to reduce electron and holes recombination • The reaction is conducted on a stirred batch annular reactor with a suspended catalyst
T. W. Woolerton *et al.* (2010)[208]	Enzyme CODHI with RuP modified TiO_2/—	—	CO_2 (98%), CH_4 (2%)/tungsten-halogen lamp (420 nm)/45 mW cm^{-2}	(293/—/6/4/—), (0.005/—/ nanoparticles/—/ suspended)	Carbon monoxide/ 250/—	• Photocatalytic reaction is carried out in a Pyrex pressure vessel (9 mL) with gentle stirring • Reaction is focused on a two-electron pathway to avoid the thermodynamically difficult step involved in one-electron CO_2 activations
C. Wang *et al.* (2010)[200]	CdSe–Pt–TiO_2/—	Wet impregnation method	CO_2 (0.0004 atm), water vapor (0.004 atm)/300 W Xe arc lamp (>420 nm)/100 mW cm^{-2}	(—/—/—/6/—), (0.3/50/ hetero-structured/—/ supported)	Methane, methanol/ 0.0019, 0.000137/—	• Quantum dot-sensitized TiO_2 heterostructured materials are proficient for photoreduction of CO_2 using visible light • Results exhibit that germane can be used on photoreduction reactions for CO_2 capture and reuse
Z. Zhao *et al.* (2009)[203]	0.7 wt% Co(II)Pc–TiO_2/—	*In situ* synthesized by advanced sol–gel method	CO_2 (—), NaOH (100 mL, 0.1 N aqueous solution)/500 W tungsten-halogen lamp/—	(—/—/—/10/—), (0.15/ 75.23/11.35 nm particle/—/suspended)	Formic acid/150/—	• The yield of *in situ* CoPc–TiO_2 is much higher than those of TiO_2 and physical absorbed CoPc–TiO_2 • Reaction is conducted in a Pyrex glass cell (100 mL) with an optical window
Z. Zhao *et al.* (2009)[204]	0.5% CoPc–TiO_2/—	Sol–gel method	CO_2 (saturated), NaOH (0.1 N,100 mL aqueous solutions)/ 500 W tungsten-halogen lamp/—	(673/—/—/6/—), (0.15/ 90.7/11.02 nm particle/ 0.1/supported)	Formic acid/57/—	• CoPc–TiO_2 prepared by sol–gel shows relatively high photocatalytic activity, compared with TiO_2 synthesized by sol–gel method • A Pyrex cell with an optical window (100 mL) is used to conduct the photocatalytic reaction

Table 7 (*Contd.*)

Researcher (year) and ref.	Catalyst composition/ band gap energy	Catalyst preparation technique	Reactants (amount)/ radiation source/ light intensity	Operating variables (T/P/pH/t/QE), physical properties (W/SA/PS/SC/MP)	Major product/Yield (μmol h^{-1} per g catalyst)/efficiency (%)	Comments
H.-C. Yang *et al.* (2009)[214]	Sensitized 45 wt% Cu–TiO_2 on SBA-15/ 3.2 eV	Sol–gel synthesis and hydrolysis–condensation process	CO_2 (saturated), NaOH (0.1 N, 550 mL aqueous solution)/400 W medium-pressure halide lamp (365 nm)/—	(315/—/7/8/—), (0.05/ 436/5.5 nm particles/—/ suspended)	Methanol/475/—	• Loading amount of TiO_2 on mesoporous SBA-15 composite photocatalysts control the crystallize size of the supported TiO_2 particles and the mesoporous structure of the catalyst
Jeffrey C. S. Wu (2009)[194]	Dye-sensitized Cu–Fe loaded on P25/—	Dip-coating method	CO_2 (saturated), water vapor (—)/sunlight (400–800 nm)/20 mW cm^{-2}	(—/—/—/—/—), (—/—/film composite/—/ supported)	Methanol/—/—	• Dye-sensitized Cu–Fe loaded on P25 photocatalyst can completely use the light energy of 400–800 nm from sunlight and significantly increase its photoactivity
Nguyen and Wu (2008)[166]	Sensitized TiO_2 with 0.5 wt% Cu–Fe loaded On SiO_2/2.95 eV	Sol–gel process	CO_2 (saturated), H_2O (—)/natural sunlight/2.05 mW cm^{-2}	348/—/—/6/0.0182), (0.5/44.7/53 nm thickness film/—/ supported)	Methane/0.279/0.0152	• An optical-fiber reactor consists of a continuous circular Pyrex glass vessel (216 cm^3) with a quartz window in which catalyst-coated optical fibers are inserted • Cu–Fe loaded on TiO_2–SiO_2–acac catalyst shows the superior photoactivity, compared with that of bare TiO_2–SiO_2–acac counterpart
Jeffrey C. S. Wu *et al.* (2008)[215]	Sensitized TiO_2 with 1 wt% Ag coated on optical fiber/3.5 eV	Thermal hydrolysis method	CO_2 (1.13 atm), H_2O (0.03 bar)/UV light (365 nm)/10 000 mW cm^{-2}	(348/—/—/11/0.00013), (—/71.66/spherical particles of 12 nm/—/ supported)	Methanol/4.1/—	• An optical-fiber photoreactor, built-in 216*x* catalyst-coated fibers are supported on circular plates and irradiated through the quartz window having a large external area of optical fiber to disperse catalysts • Optical-fiber delivers a medium to transmit light uniformly throughout the reactor compared with a traditional packed-bed reactor
The V. Nguyen *et al.* (2008)[195]	N3 dye–0.5 wt% Cu–0.5 wt% Fe–TiO_2/3.11 eV	Dip-coating method	CO_2 (saturated), water vapor (—)/sunlight/20 mW cm^{-2}	(348/—/—/6/—), (—/48.7/film composite/—/ supported)	Methane/0.617/—	• A continuous circular Pyrex glass (216 cm^3) optical fiber photoreactor is irradiated by concentrated sunlight through a quartz window • N3-dye highly increases the photoactivity under concentrated natural sunlight and delivers efficient charge transfer
Z. Zhao *et al.* (2007)[205]	1 wt% Zn(II)Pc–TiO_2/—	Sol–gel method and *in situ* chemical synthesis technique	CO_2 (saturated), NaOH (100 mL, 0.1 N aqueous solution)/500 W tungsten-halogen lamp/—	(—/—/—/10/—), (0.15/—/28 nm particle/—/suspended)	Formic acid/98/0.37	• Results show that formic acid production is significantly increased by loading ZnPc, and having a higher selectivity than metal catalysts for the reduction of CO_2 • A magnetic stirred Pyrex glass cell (100 mL) with an optical window is used to carry out the reaction

Table 7 (*Contd.*)

Researcher (year) and ref.	Catalyst composition/ band gap energy	Catalyst preparation technique	Reactants (amount)/ radiation source/ light intensity	Operating variables (T/P/pH/t/QE), physical properties (W/SA/PS/SC/MP)	Major product/Yield (μmol h^{-1} per g catalyst)/efficiency (%)	Comments
O. Ozcan *et al.* (2007)[196]	BrGly-pt loaded on TiO_2/—	Dip-coat sol–gel technique and wet impregnation method	CO_2 (0.88 atm), water vapor (0.03 atm)/75 W daylight lamp/58 mW cm^{-2}	(—/0.9/—/3/0.0228), (—/—/>1 μm thick film composite/—/ supported)	Methane/0.2/—	• Perylene di-imide derivatives are used to show light harvesting capability similar to the tris(2,2-bipyridyl) ruthenium(II) chloride hexahydrate • The reaction is conducted on a glass chamber connected to a vacuum line • It is found that visible light performances of the dyes are in the following order in the presence of Pt: Rubpy > BrAsp > BrGly
Tseng and Wu (2004)[216]	Sensitized TiO_2 with 2 wt% Cu/—	Sol–gel procedures and post-treatments	CO_2 (saturated), NaOH (0.2 N aqueous solution)/ Hg lamp (254 nm)/—	(—/—/7/30/—), (0.3/—/ 25 nm particle/—/ suspended)	Methanol/17/—	• It is found that photoactivity declines when Cu(I) changes to Cu (0) or aggregates after reduction with H_2 • Reaction is carried out in a cylindrical quartz reactor with a capacity of 300 mL • It is identified that the photoactivity of Ag–TiO_2 is lower than those of Cu–TiO_2 due to the strong affinity between Ag clusters and photoelectrons
Hirose *et al.* (2003)[198]	$Co(bpy)_3^{2+}$ sensitized with $Ru(bpy)_3^{2+}$ supported on Nafion film/—	Laboratory preparation	CO_2 (saturated), DMF & TEOA (30 mL solution)/Xe lamp/—	(—/1/<1/46/—), (0.1/—/ particles on polymer film/—/supported)	Carbon monoxide/ 25[d]/—	• Long catalytic activity is observed for more than 400 h under atmospheric pressure • A gastight photolysis photoreaction vessel (Pyrex) is used to conduct the reaction • This system permits easy handling and recovery of the Ru complex including repeated cycles using CO_2 refreshing
Ishitani *et al.* (1993)[147]	Sensitized TiO_2 (Degussa P-25) particles with 2% wt Pd/8.34 eV	Photochemical deposition method	CO_2 (saturated), H_2O (1.5 mL)/500 W high pressure Hg lamp (310 nm)/—	(278/0.86/—/5/—), (0.15/—/powder/—/ suspended)	Methane/0.3/—	• It is suggested that product distribution is dependent on the sort of metal on the surface of TiO_2 • Degassed quartz vessel is used to carry out the photoreduction
Thampi *et al.* (1987)[217]	25% Ru −75% RuO_x sensitized on TiO_2/3 eV	Laboratory preparation	CO_2 (0.05 atm, 1 mL), H_2 (0.6 atm, 12 mL)/150 W high pressure Xe lamp (310–435 nm)/—	(298/1/—/5/0.59), (0.1/ 55/spherical shape particle/3.8/suspended)	Methane/0.5[e]/—	• Photocatalysts are kept on the bottom of a flat Pyrex vessel (20 cm^3) with a side arm and septum • Elevated temperature and pressure play an important role in advancing the reaction rate and yields
Lehn and Ziessel (1982)[197]	Ru-bipyridine-Co(II) chloride/—	Standard laboratory synthesis	CO_2 (700 mL), H_2O (6 mL)/1000 W Xe or Hg ozone-free oriel lamp (400 nm)/—	(303/1/8.5/26/—), (—/—/—/—/suspended)	Carbon monoxide/ 25[d]/—	• It has been observed that addition of free bipyridine intensely decreases CO generation but increases H_2 production • The photocatalytic reaction is carried out in a 50 mL round-bottom flask

[a] T/P/pH/t/QE: temperature (K)/pressure (atm)/pH/illumination period (hours)/quantum efficiency (%). W/SA/PS/SC/MP: weight of photocatalyst (g)/surface area (m^2 g^{-1})/photocatalyst structure (diameter)/semiconductor concentration (g mL^{-1})/mode of photocatalyst. '—': not mentioned in the original paper. [b] ppm h^{-1} g^{-1} catalyst. [c] μmol m^{-2} catalyst. [d] μmol. [e] mmol.

this study, visible light performance of the dyes was in the following order in presence of Pt: Rubpy > BrAsp > BrGly.

Much attention has been given to $[Ru(bpy)_3]^{2+}$ cation because of its unique optical features. The combination of $[Ru(bpy)_3]^{2+}$ and cobalt(II) chloride has been investigated over CO_2 photoreduction, where Ru and Co complexes act as a photosensitizer and a catalyst, respectively.[197] Absorbing photon energy, the $[Ru(bpy)_3]^{2+}$ cation transforms to the triplet state, denoted by $[Ru(bpy)_3]^{2+}$*. It was observed that the extra addition of bipyridine intensely reduced CO formation but raised the H_2 yield. On the other hand, cobalt(II) chloride acts as an effective mediator for both CO and H_2 productions and highly endorses CO yield. $Co(bpy)_3{}^{2+}$ sensitized with $Ru(bpy)_3{}^{2+}$ supported on a cation exchange Nafion film has been synthesized to carry out the photocatalytic reduction of CO_2 for a period of more than 400 h under atmospheric pressure.[198] High stability of the metal complexes is obtained by the suppression of the decomposition of the Ru complex fixed on the polymer surface. In this system, $[Ru(bpy)_3]^{2+}$ was immobile on a cation exchange polymer and $[Co(bpy)_3]^{2+}$ was mixed in a di-methylformamide (DMF) and triethanol amine (TEOA) as a solvent and reducing agent, respectively. It is assumed that the photoinduced Ru complex transmits an electron to Co(II) complex, which acts as a reaction medium of CO_2, and at that time, a tertiary amine (sacrifice reagent) reduced the oxidized Ru(III) complex.[198]

2.4.2 Quantum dots (QDs)-sensitized photocatalysts. A quantum dot-sensitized photocatalyst is one of the advanced approaches in photochemical conversion of CO_2 because of its intrinsic optical and electrical behavior. These characteristics are strongly influenced by the size of quantum dots materials. Generally, chalcogenide metals (including CdSe or ZnS) are used with the semiconductors to facilitate the photon transformation of CO_2 into hydrocarbon fuels. In Section 2.2.1, there is a brief discussion about the metal sulfide (CdS and ZnS) semiconductors, which also have such unique optical properties as quantum dots materials. To understand the size reliance on the photochemical reduction of CO_2, Wang *et al.* developed a PbS QDs-sensitized Cu–TiO_2 catalyst of three different sizes of PbS QDs samples (3 nm, 4 nm and 5 nm).[199] Among them, 4 nm PbS QD-sensitized Cu–TiO_2 displayed the maximum CO_2 transformation rate due to the absorption of visible spectrum ($\lambda > 610$ nm) and charge separation properties. It is found that small-sized dots can facilitate the blue edge of the spectrum, while the large-sized dot is closer to the red edge spectrum. Particularly, small-sized QDs inject electrons swiftly to the conduction band edge of TiO_2 and large-sized QDs cover the visible region.[200] Moreover, the electron transfer rate was very fast (less than 1 ns) from the excited PbS QDs state to the TiO_2 conduction band state.[201] Another investigation was conducted on the CdSe QDs-sensitized Pt–TiO_2 composite heterostructure, which revealed a response to the visible light region ($\lambda > 420$ nm).[200]

2.4.3 Phthalocyanine sensitized photocatalysts. For visible light irradiation, metal phthalocyanines are also applied in CO_2 photoreduction, which have outstanding semi-conductivity and chemical stability.[202] The CoPc–TiO_2 nanocomposites are characterized by Zhao *et al.*[203,204] It was observed that excited CoPc molecules emitted the electrons to the conduction band of TiO_2 during visible light irradiation; this phenomenon then improved the electron–hole separation process to increase the photocatalytic efficiency. From Table 7, it is found that the incorporation of 0.7% CoPc into TiO_2 exhibited a high yield rate of formic acid (about 150 μmol g^{-1} h^{-1}) than that of 0.5% CoPc addition to TiO_2. In addition, their investigation was conducted on ZnPc–TiO_2 and found that ZnPc has a higher selectivity of formic acid than metal catalysts by decreasing the recombination possibility of the hole–electron pairs.[205] It is important that the excess loading of ZnPc can reduce the photocatalytic activity because the active TiO_2 surface sites can be blocked by additional metal phthalocyanines, and the optimal amount is observed, 1.0 wt% ZnPc. However, according to the observation by Wang *et al.*, the band gap of TiO_2 can be minimized from 2.95 eV (at 0.6 wt% ZnPc) to 2.79 eV by loading 5 wt% ZnPc.[206]

2.4.4 Other photosensitizers. Enzymes have an effective sensitization facility to the red shift of TiO_2, compared with other sensitizers.[207] Woolerton *et al.* handled carboxydothermus hydrogenoformans (Ch)-derived carbon monoxide dehydrogenases (CODHI) enzyme to functionalize the RuP-sensitized TiO_2 nanoparticles for CO_2 photoexcitation.[208,209] Anaerobic organisms, Ch contains five forms of CODH enzymes, each having active sites of [Ni4Fe-4S]. The subunit of these enzymes (Ni–CODHs) possesses a buried active site that is attached to the protein exterior by a chain of [4Fe-4S] clusters. Electrons can easily access or leave the enzyme by distal cluster (D-cluster) that is joined between the two subunits. In this experiment, visible light-excited RuP sensitizer nanoparticles transfer photoinduced electrons to TiO_2 for easing its solar light activation.[209,210] These electrons can easily get into the CODH enzyme through the D-cluster and also move through a second [4Fe–4S] cluster to the active site where the CO_2 reduction has taken place.

Recently, co-loaded novel metals are using the semiconductor catalysts as photosensitizers. For example, sensitized TiO_2 film with Au nanoparticles is modified by Hou *et al.* for turning CO_2 into fuels.[211] Here, Au nanoparticles are photoexcited by the plasmon effect (the generation of robust electric fields by surface plasmon resonance of the Au nanoparticle), which shifts the photoinduced electrons from the Au to the TiO_2. Another approach of sensitized TiO_2 with Cu on supportive SiO_2 is applied in terms of solar fuel production from CO_2.[77,212]

2.5 Flexible substrate based photocatalysts

In photochemical reactions, the involvement of flexible substrates have generated interest because they deliver a high surface area for catalysts on the film of substrates such as polyethyleneterphthalate (PET), polyethylenenaphtalate (PEN), polyethylene (PE) and polypropylene (PP).[218] However, the degradation of polymer substrates by solar irradiation depends on the operating period of atmospheric exposure.[219] This photodegradation is carried out by a combination of photolysis and photocatalytic oxidation.[218] The formation of volatile products due to photodegradation is another limitation in the case of polymeric substrates.[220] Table 8 represents the full information

Table 8 Advances in flexible substrate catalysts for CO_2 photoreduction[a]

Researcher (year) and ref.	Catalyst composition/ band gap energy	Catalyst preparation technique	Reactants (amount)/ radiation source/ light intensity	Operating variables (T/P/pH/t/QE), physical properties (W/SA/PS/SC/MP)	Major product/yield (μmol h^{-1} per g catalyst)/selectivity (%)	Comments
W. Kim *et al.* (2012)[223]	Nafion layer on 1.0 wt % Pd-deposited TiO_2/—	Laboratory synthesis	CO_2 (saturated), H_2O (—)/UV light (>300 nm)/—	(—/—/3/5/—), (—/—/nanoparticle/ 1.5×10^{-6}/ suspended)	Methane/7.6[b]/—	• Nafion layer enhances proton-coupled, multiple-electron transfer reactions, stabilizes intermediates and inhibits the re-oxidation of the CO_2 reduction products by increasing the local proton activity within the layer • Palladium is selected to retard the recombination of H atoms to minimize the production of H_2
J. Jensen *et al.* (2011)[218]	TiO_2–PET/—	Spray coating	CO_2 (25 mol), H_2 (75 mol)/Osram light bulb/120 mW cm^{-2}	(308/—/—/230/—), (—/—/film with 130 μm thickness/—/ supported)	Carbon monoxide/ 0.0013/—	• Polymer substrates are applied in this study with high-active area of 100 cm^2 enable to achieve catalyst-covered film within a short time and at a reasonable production cost • UV degradation of polymer substrates (photocatalytic oxidation) can be suppressed, but not avoided, by using oxygen-free conditions
T. Arai *et al.* (2011)[224]	Cu_2ZnSnS_4 modified by ruthenium complex polymer/1.5 eV	Chemical polymerization method	CO_2 (saturated), H_2O (—)/visible light irradiation (200–400 nm)/—	(—/—/—/3/—), (—/—/photocathode/ —/supported)	Formic acid/0.49[c]/> 80	• Sulfide semiconductor that shows a narrow band gap with high selectivity in photoelectrochemical CO_2 reduction • The insertion of Se into the catalyst enhances hole mobility and increases the photocurrent
Hirose *et al.* (2003)[198]	$Co(bpy)_3^{2+}$ with $Ru(bpy)_3^{2+}$ supported on Nafion film/—	Laboratory preparation	CO_2 (saturated), DMF with TEOA (30 mL solution)/Xe lamp/—	(—/1/< 1/46/—), (1/—/ particles on polymer film/—/supported)	Carbon monoxide/ 25[b]/—	• Catalytic activity shows more than 400 h under atmospheric pressure • Photoreaction is carried out in a gastight photolysis photoreaction vessel (Pyrex) • This system allows easy handling and recovery of the Ru complex with repeated cycles, using CO_2 refreshing

[a] T/P/pH/t/QE: temperature (K)/pressure (atm)/pH/illumination period (hours)/quantum efficiency (%). W/SA/PS/SC/MP: weight of photocatalyst (g)/surface area (m^2 g^{-1})/photocatalyst structure (diameter)/semiconductor concentration (g mL^{-1})/mode of photocatalyst. '—': not mentioned in the original paper. [b] μmol. [c] mM.

of flexible substrate based photocatalysts, which are gathered from important investigations related to CO_2 photoconversion.

Some aromatic polyesters such as PET, PEN and similar flexible substrates act in different ways under light irradiation, compared with olefins (PE and PP). Aromatic polyesters are able to absorb light with a long wavelength (<330 nm) due to the aromatic rings of carbonyl groups.[220] Another important factor is the oxygen diffusion constant of flexible substrates. Higher oxygen diffusion constants may lead to oxidation in all parts of the surface.[221] Comparatively, polymer degradation is lesser on the surface of the PET because of its restriction to diffuse oxygen, whereas the diffusion is higher in the PE.[218,221,222]

Use of a Nafion (perfluorinated polymers with sulfonate groups) thin film on Pd-loaded TiO_2 nanoparticles was introduced by Kim *et al.* due to its stability against photocatalytic oxidation, and hence increases the photochemical conversion of CO_2 under visible light irradiation.[223] To provide multiple electrons, the Nafion layer can increase local proton activity inside the layer. It also helps to stabilize the intermediates and prevent the re-oxidation of the CO_2 reduction yields because it inhibits direct interaction between products and surfaces of the catalysts. Another investigation shows that Nafion film acts as a good supportive material for catalysts due to cation exchange ability.[198] This Nafion-supported $Co(bpy)_3^{2+}$ and $Ru(bpy)_3^{2+}$ system can increase the catalytic activity to a maximum of 400 h in atmospheric condition because of obstruction to the breakdown of $[Ru(bpy)_3]^{2+}$ complexes that are trapped on the cation exchange polymer surface, and hence the separation of ligands is minimized. Low-band gap (1.5 eV) Cu_2ZnSnS_4 modified by the ruthenium complex polymer is a new addition to determine the photochemical performance of CO_2 reduction under the visible light region, which shows high selectivity of the formate (>80%).[224]

3. Conclusions

The transformation of CO_2 towards hydrocarbon fuels is a substitute approach to regulate both fuel crisis and global warming. Various inquiries have been undertaken to evaluate the photocatalytic performance over CO_2 transformation into hydrocarbon fuels. This technology was found to be more promising, compared with other approaches such as thermochemical, electrochemical, and biological transformation technologies. In this paper, a general overview is emphasized on the behavior of different types of photocatalysts with respect to CO_2 transformation into fuel. In various investigations, it was observed that most of the studies were carried out in the presence of artificial light sources. Recently, researchers have focused on direct solar fuel production by CO_2 conversion. For such a phenomenon, the selective catalysts must have the desired band gap energy for visible light response. Previously, unmodified oxide and non-oxide semiconductors are widely used with or without supportive materials in this technology. However, some of them have high band gap energy and low conversion yields. To facilitate, some techniques have been followed to minimize band gap energy by doping the semiconductors with foreign elements like novel metals, transition metals, co-metals, and non-metals. It also influences the charge transfer rate and reduces the electron–hole recombination. Further, different substrate materials were used to achieve high surface area and the catalysts' immobilization during the photocatalytic irradiation. Recently, different types of sensitization techniques are incorporated to improve the photocatalytic performance under visible light irradiation like dye sensitization, enzyme-based sensitization, QDs sensitization, and phthalocyanine sensitization. Both doped and sensitized semiconductors were employed for higher conversion. The selectivity of products not only depends on the catalysts' compositions but also on the choice of reductant and the solvent used in the catalytic system. Besides water, organic sacrificial reducing reagents are the most common reductants used in the photochemical CO_2 conversion process. Although water is available and affordable, there are some limitations like low CO_2 solubility, resulting in water splitting rather than CO_2 reduction. Instead, methane and hydrogen were used as significant reductants in many investigations reported in this review. Other factors are definitely considerable for evaluating photocatalytic performance on CO_2 reduction such as catalysts' dosage, reactants' ratio, reaction temperature, time, system pressure, pH, light intensity and wavelength. A clear idea is essential for understanding the reaction mechanisms together with charge carrier dynamics within the catalysts and at their interfaces with the metal co-catalysts. From this review, it is clear that the existing techniques are insufficient to make them applicable for the industrial production of fuels. As a result, the selection of solar-driven photocatalysts is essential for industrial solar fuel harvesting from CO_2.

Acknowledgements

The authors acknowledge financial support from project RP015/2012D and D000011-16001, Center of Research Grant Management, University of Malaya, 50603 Kuala Lumpur, Malaysia.

References

1 S. C. Roy, O. K. Varghese, M. Paulose and C. A. Grimes, *ACS Nano*, 2010, **4**, 1259–1278.
2 L. T. H. Nam, T. Q. Vinh, N. T. T. Loan, V. D. S. Tho, X.-Y. Yang and B.-L. Su, *Fuel*, 2011, **90**, 1069–1075.
3 H. Balat and E. Kırtay, *Int. J. Hydrogen Energy*, 2010, **35**, 7416–7426.
4 T. R. Cook, D. K. Dogutan, S. Y. Reece, Y. Surendranath, T. S. Teets and D. G. Nocera, *Chem. Rev.*, 2010, **110**, 6474–6502.
5 Independent Statistics and Analysis, U.S. Energy Information Administration, 2012, retrieved from http://www.eia.gov/cfapps/ipdbproject/IEDIndex3.cfm?tid=44&pid=44&aid=2.
6 L. Jaeglé, L. Steinberger, R. V. Martin and K. Chance, *Faraday Discuss.*, 2005, **130**, 407–423.
7 BP: Statistical Review of World Energy, London, 2013, retrieved from http://www.bp.com/content/dam/bp/pdf/statistical-review/statistical_ review_of_world_energy_2013.pdf.

8 G. Shafiullah, M. Amanullah, A. Shawkat Ali, D. Jarvis and P. Wolfs, *Renewable Energy*, 2012, **39**, 183–197.
9 N. Panwar, S. Kaushik and S. Kothari, *Renewable Sustainable Energy Rev.*, 2011, **15**, 1513–1524.
10 S. Mekhilef, S. Siga and R. Saidur, *Renewable Sustainable Energy Rev.*, 2011, **15**, 1937–1949.
11 S. Dutta, *RSC Adv.*, 2012, **2**, 12575–12593.
12 G. Centi and R. A. van Santen, *Catalysis for renewables*, Wiley, Weinheim, 2008.
13 M. Dittmar, *Energy*, 2012, **37**, 35–40.
14 N. H. Afgan, *Thermal Science*, 2013, **17**, 305–321.
15 H. Li, Y. Dai, M. Köhler and R. Wang, *Energy Convers. Manage.*, 2013, **67**, 309–317.
16 T. C. Corbiere, D. Ressnig, C. Giordano and M. Antonietti, *RSC Adv.*, 2013, **3**, 15337–15343.
17 N. Y. Mansouri, R. J. Crookes and T. Korakianitis, *Energy Policy*, 2013, **63**, 681–695.
18 M. Sun, W. Fu, Q. Li, G. Yin, K. Chi, J. Ma, L. Yang, Y. Mu, Y. Chen and S. Su, *RSC Adv.*, 2014, **4**, 7178–7184.
19 M. Jamel, A. Abd Rahman and A. Shamsuddin, *Renewable Sustainable Energy Rev.*, 2013, **20**, 71–81.
20 J. Lee, H. Back, J. Kong, H. Kang, S. Suhee, S. Hongsuk, S.-O. Kang and K. Lee, *Energy Environ. Sci.*, 2013, **6**, 1152–1157.
21 V. Kaltenhauser, T. Rath, M. Edler, A. Reichmann and G. Trimmel, *RSC Adv.*, 2013, **3**, 18643–18650.
22 C. Liu, N. P. Dasgupta and P. Yang, *Chem. Mater.*, 2014, **26**, 415–422.
23 K. Sivula, *J. Phys. Chem. Lett.*, 2013, **4**, 1624–1633.
24 Y.-K. Hsu, C.-H. Yu, Y.-C. Chen and Y.-G. Lin, *RSC Adv.*, 2012, **2**, 12455–12459.
25 A. A. Lacis, G. A. Schmidt, D. Rind and R. A. Ruedy, *Science*, 2010, **330**, 356–359.
26 S. D. Kenarsari, D. Yang, G. Jiang, S. Zhang, J. Wang, A. G. Russell, Q. Wei and M. Fan, *RSC Adv.*, 2013, **3**, 22739–22773.
27 G. Xiao, P. Xiao, S. Lee and P. A. Webley, *RSC Adv.*, 2012, **2**, 5291–5297.
28 International Energy Agency Annual Report, 2012, retrieved from http://www.iea.org/publications/freepublications/publication/English.pdf.
29 I. Omae, *Coord. Chem. Rev.*, 2012, **256**, 1384–1405.
30 U.S. Department of Energy (DOE), 2013, retrieved from www.doe.gov/.
31 W.-J. Ong, M. M. Gui, S.-P. Chai and A. R. Mohamed, *RSC Adv.*, 2013, **3**, 4505–4509.
32 K. Mori, H. Yamashita and M. Anpo, *RSC Adv.*, 2012, **2**, 3165–3172.
33 X.-J. Lv, W.-F. Fu, C.-Y. Hu, Y. Chen and W.-B. Zhou, *RSC Adv.*, 2013, **3**, 1753–1757.
34 T. Sakakura, J.-C. Choi and H. Yasuda, *Chem. Rev.*, 2007, **107**, 2365–2387.
35 S. N. Habisreutinger, L. Schmidt-Mende and J. K. Stolarczyk, *Angew. Chem., Int. Ed.*, 2013, **52**, 7372–7408.
36 Z. Zou, J. Ye, K. Sayama and H. Arakawa, *Nature*, 2001, **414**, 625–627.
37 M. Ni, M. K. Leung, D. Y. Leung and K. Sumathy, *Renewable Sustainable Energy Rev.*, 2007, **11**, 401–425.
38 F. Han, V. S. R. Kambala, M. Srinivasan, D. Rajarathnam and R. Naidu, *Appl. Catal., A*, 2009, **359**, 25–40.
39 D. Bahnemann, *Sol. Energy*, 2004, **77**, 445–459.
40 R. Benedix, F. Dehn, J. Quaas and M. Orgass, *Lacer*, 2000, **5**, 157–168.
41 A. Fujishima, T. N. Rao and D. A. Tryk, *J. Photochem. Photobiol., C*, 2000, **1**, 1–21.
42 T. Inoue, A. Fujishima, S. Konishi and K. Honda, *Nature*, 1979, **277**, 637–638.
43 S. Sakthivel and H. Kisch, *Angew. Chem., Int. Ed.*, 2003, **42**, 4908–4911.
44 H. Tada, Q. Jin, H. Nishijima, H. Yamamoto, M. Fujishima, S. i. Okuoka, T. Hattori, Y. Sumida and H. Kobayashi, *Angew. Chem., Int. Ed.*, 2011, **123**, 3563–3567.
45 M. Tahir and N. S. Amin, *Appl. Catal., B*, 2013, **142–143**, 512–522.
46 R. Van Grieken, J. Aguado, M. López-Muñoz and J. Marugán, *J. Photochem. Photobiol., A*, 2002, **148**, 315–322.
47 P. Bouras, E. Stathatos and P. Lianos, *Appl. Catal., B*, 2007, **73**, 51–59.
48 K. Kočí, L. Obalová, L. Matějová, D. Plachá, Z. Lacný, J. Jirkovský and O. Šolcová, *Appl. Catal., B*, 2009, **89**, 494–502.
49 K. Kočí, L. Obalová and Z. Lacný, *Chem. Pap.*, 2008, **62**, 1–9.
50 S. S. Tan, L. Zou and E. Hu, *Catal. Today*, 2006, **115**, 269–273.
51 G. P. Fotou and S. E. Pratsinis, *Chem. Eng. Commun.*, 1996, **151**, 251–269.
52 T. Yui, A. Kan, C. Saitoh, K. Koike, T. Ibusuki and O. Ishitani, *ACS Appl. Mater. Interfaces*, 2011, **3**, 2594–2600.
53 N. M. Dimitrijevic, B. K. Vijayan, O. G. Poluektov, T. Rajh, K. A. Gray, H. He and P. Zapol, *J. Am. Chem. Soc.*, 2011, **133**, 3964–3971.
54 S. Kaneco, H. Kurimoto, Y. Shimizu, K. Ohta and T. Mizuno, *Energy*, 1999, **24**, 21–30.
55 S. Kaneco, H. Kurimoto, K. Ohta, T. Mizuno and A. Saji, *J. Photochem. Photobiol., A*, 1997, **109**, 59–63.
56 G. Dey, A. Belapurkar and K. Kishore, *J. Photochem. Photobiol., A*, 2004, **163**, 503–508.
57 G. Li, L. Li, J. Boerio-Goates and B. F. Woodfield, *J. Am. Chem. Soc.*, 2005, **127**, 8659–8666.
58 G. Xi, S. Ouyang, P. Li, J. Ye, Q. Ma, N. Su, H. Bai and C. Wang, *Angew. Chem., Int. Ed.*, 2012, **51**, 2395–2399.
59 L. Yuliati, H. Itoh and H. Yoshida, *Chem. Phys. Lett.*, 2008, **452**, 178–182.
60 Y. Kohno, T. Tanaka, T. Funabiki and S. Yoshida, *Phys. Chem. Chem. Phys.*, 2000, **2**, 5302–5307.
61 K. Teramura, T. Tanaka, H. Ishikawa, Y. Kohno and T. Funabiki, *J. Phys. Chem. B*, 2004, **108**, 346–354.
62 C.-C. Lo, C.-H. Hung, C.-S. Yuan and J.-F. Wu, *Sol. Energy Mater. Sol. Cells*, 2007, **91**, 1765–1774.
63 Y. Liu, B. Huang, Y. Dai, X. Zhang, X. Qin, M. Jiang and M.-H. Whangbo, *Catal. Commun.*, 2009, **11**, 210–213.
64 J. Yu and A. Kudo, *Adv. Funct. Mater.*, 2006, **16**, 2163–2169.

65 Y. Zhou, Z. Tian, Z. Zhao, Q. Liu, J. Kou, X. Chen, J. Gao, S. Yan and Z. Zou, *ACS Appl. Mater. Interfaces*, 2011, **3**, 3594–3601.
66 Q. Liu, Y. Zhou, J. Kou, X. Chen, Z. Tian, J. Gao, S. Yan and Z. Zou, *J. Am. Chem. Soc.*, 2010, **132**, 14385–14387.
67 X. Li, H. Pan, W. Li and Z. Zhuang, *Appl. Catal., A*, 2012, **413**, 103–108.
68 M. Stock and S. Dunn, *Ferroelectrics*, 2011, **419**, 9–13.
69 J. W. Lekse, M. K. Underwood, J. P. Lewis and C. Matranga, *J. Phys. Chem. C*, 2012, **116**, 1865–1872.
70 X.-H. Xia, Z.-J. Jia, Y. Yu, Y. Liang, Z. Wang and L.-L. Ma, *Carbon*, 2007, **45**, 717–721.
71 A. Yahaya, M. Gondal and A. Hameed, *Chem. Phys. Lett.*, 2004, **400**, 206–212.
72 M. Anpo, H. Yamashita, Y. Ichihashi and S. Ehara, *J. Electroanal. Chem.*, 1995, **396**, 21–26.
73 F. Solymosi and I. Tombacz, *Catal. Lett.*, 1994, **27**, 61–65.
74 H. Jüntgen, *Fuel*, 1986, **65**, 1436–1446.
75 M. Kruk, M. Jaroniec, C. H. Ko and R. Ryoo, *Chem. Mater.*, 2000, **12**, 1961–1968.
76 M.-J. López-Muñoz, R. v. Grieken, J. Aguado and J. Marugán, *Catal. Today*, 2005, **101**, 307–314.
77 Y. Li, W.-N. Wang, Z. Zhan, M.-H. Woo, C.-Y. Wu and P. Biswas, *Appl. Catal., B*, 2010, **100**, 386–392.
78 B.-J. Liu, T. Torimoto and H. Yoneyama, *J. Photochem. Photobiol., A*, 1998, **115**, 227–230.
79 N. Gokon, N. Hasegawa, H. Kaneko, H. Aoki, Y. Tamaura and M. Kitamura, *Sol. Energy Mater. Sol. Cells*, 2003, **80**, 335–341.
80 J. Papp, S. Soled, K. Dwight and A. Wold, *Chem. Mater.*, 1994, **6**, 496–500.
81 M. Subrahmanyam, S. Kaneco and N. Alonso-Vante, *Appl. Catal., B*, 1999, **23**, 169–174.
82 M. Anpo, H. Yamashita, Y. Ichihashi, Y. Fujii and M. Honda, *J. Phys. Chem. B*, 1997, **101**, 2632–2636.
83 Q. D. Truong, J.-Y. Liu, C.-C. Chung and Y.-C. Ling, *Catal. Commun.*, 2012, **19**, 85–89.
84 R. A. H. W. A. Deer and J. Zussman, *An introduction to the rock-forming minerals*, Harlow, Longman, 2nd edn, 1992.
85 K. Kočí, V. Matějka, P. Kovář, Z. Lacný and L. Obalová, *Catal. Today*, 2011, **161**, 105–109.
86 M. A. Asi, C. He, M. Su, D. Xia, L. Lin, H. Deng, Y. Xiong, R. Qiu and X.-z. Li, *Catal. Today*, 2011, **175**, 256–263.
87 J. Popić, M. Avramov-Ivić and N. Vuković, *J. Electroanal. Chem.*, 1997, **421**, 105–110.
88 J. Qu, X. Zhang, Y. Wang and C. Xie, *Electrochim. Acta*, 2005, **50**, 3576–3580.
89 T.-f. Xie, D.-j. Wang, L.-j. Zhu, T.-j. Li and Y.-j. Xu, *Mater. Chem. Phys.*, 2001, **70**, 103–106.
90 K. Ogura, M. Kawano, J. Yano and Y. Sakata, *J. Photochem. Photobiol., A*, 1992, **66**, 91–97.
91 H. W. Nasution, E. Purnama, S. Kosela and J. Gunlazuardi, *Catal. Commun.*, 2005, **6**, 313–319.
92 S. Qin, F. Xin, Y. Liu, X. Yin and W. Ma, *J. Colloid Interface Sci.*, 2011, **356**, 257–261.
93 P.-Y. Liou, S.-C. Chen, J. C. Wu, D. Liu, S. Mackintosh, M. Maroto-Valer and R. Linforth, *Energy Environ. Sci.*, 2011, **4**, 1487–1494.
94 P.-W. Pan and Y.-W. Chen, *Catal. Commun.*, 2007, **8**, 1546–1549.
95 D.-S. Lee, H.-J. Chen and Y.-W. Chen, *J. Phys. Chem. Solids*, 2012, **73**, 661–669.
96 P. Usubharatana, D. McMartin, A. Veawab and P. Tontiwachwuthikul, *Ind. Eng. Chem. Res.*, 2006, **45**, 2558–2568.
97 W. Wang and Y. Ku, *J. Photochem. Photobiol., A*, 2003, **159**, 47–59.
98 S. Yan, L. Wan, Z. Li and Z. Zou, *Chem. Commun.*, 2011, **47**, 5632–5634.
99 Q. Liu, Y. Zhou, Z. Tian, X. Chen, J. Gao and Z. Zou, *J. Mater. Chem.*, 2012, **22**, 2033–2038.
100 A. Kudo and Y. Miseki, *Chem. Soc. Rev.*, 2009, **38**, 253–278.
101 K. Maeda and K. Domen, *J. Phys. Chem. C*, 2007, **111**, 7851–7861.
102 X. Chen, S. Shen, L. Guo and S. S. Mao, *Chem. Rev.*, 2010, **110**, 6503–6570.
103 H. Tong, S. Ouyang, Y. Bi, N. Umezawa, M. Oshikiri and J. Ye, *Adv. Mater.*, 2012, **24**, 229–251.
104 K. Zhang and L. Guo, *Catal. Sci. Technol.*, 2013, **3**, 1672–1690.
105 I. Tsuji, H. Kato and A. Kudo, *Chem. Mater.*, 2006, **18**, 1969–1975.
106 H. Fujiwara, H. Hosokawa, K. Murakoshi, Y. Wada and S. Yanagida, *Langmuir*, 1998, **14**, 5154–5159.
107 O. Kozák, P. Praus, K. Kočí and M. Klementová, *J. Colloid Interface Sci.*, 2010, **352**, 244–251.
108 K. Kočí, M. Reli, O. Kozák, Z. Lacný, D. Plachá, P. Praus and L. Obalová, *Catal. Today*, 2011, **176**, 212–214.
109 P. Johne and H. Kisch, *J. Photochem. Photobiol., A*, 1997, **111**, 223–228.
110 P. Praus, O. Kozák, K. Kočí, A. Panáček and R. Dvorský, *J. Colloid Interface Sci.*, 2011, **360**, 574–579.
111 B. R. Eggins, P. K. Robertson, E. P. Murphy, E. Woods and J. T. Irvine, *J. Photochem. Photobiol., A*, 1998, **118**, 31–40.
112 B.-J. Liu, T. Torimoto and H. Yoneyama, *J. Photochem. Photobiol., A*, 1998, **113**, 93–97.
113 H. Fujiwara, H. Hosokawa, K. Murakoshi, Y. Wada, S. Yanagida, T. Okada and H. Kobayashi, *J. Phys. Chem. B*, 1997, **101**, 8270–8278.
114 C. Amatore and J. M. Saveant, *J. Am. Chem. Soc.*, 1981, **103**, 5021–5023.
115 J. Yuan, C. Zhang, C. Li, M. Chen and W. Shangguan, *MRS Proceedings*, Cambridge Univ. Press, 2011, p. 1326.
116 X. Li, J. Chen, H. Li, J. Li, Y. Xu, Y. Liu and J. Zhou, *J. Nat. Gas Chem.*, 2011, **20**, 413–417.
117 H. Inoue, H. Moriwaki, K. Maeda and H. Yoneyama, *J. Photochem. Photobiol., A*, 1995, **86**, 191–196.
118 X. V. Zhang, S. T. Martin, C. M. Friend, M. A. Schoonen and H. D. Holland, *J. Am. Chem. Soc.*, 2004, **126**, 11247–11253.
119 M. Halmann, *Nature*, 1978, **275**, 115–116.
120 S. Kaneco, H. Katsumata, T. Suzuki and K. Ohta, *Chem. Eng. J.*, 2006, **116**, 227–231.

121 E. E. Barton, D. M. Rampulla and A. B. Bocarsly, *J. Am. Chem. Soc.*, 2008, **130**, 6342–6344.
122 K. Hirota, D. A. Tryk, T. Yamamoto, K. Hashimoto, M. Okawa and A. Fujishima, *J. Phys. Chem. B*, 1998, **102**, 9834–9843.
123 B. A. Parkinson and P. F. Weaver, *Nature*, 1984, **309**, 148–149.
124 B. Aurian-Blajeni, M. Halmann and J. Manassen, *Sol. Energy Mater.*, 1983, **8**, 425–440.
125 R. Hinogami, Y. Nakamura, S. Yae and Y. Nakato, *J. Phys. Chem. B*, 1998, **102**, 974–980.
126 R. L. Cook, R. C. MacDuff and A. F. Sammells, *J. Electrochem. Soc.*, 1988, **135**, 3069–3070.
127 Y. Shioya, K. Ikeue, M. Ogawa and M. Anpo, *Appl. Catal., A*, 2003, **254**, 251–259.
128 K. Ikeue, S. Nozaki, M. Ogawa and M. Anpo, *Catal. Today*, 2002, **74**, 241–248.
129 K. Ikeue, H. Yamashita, M. Anpo and T. Takewaki, *J. Phys. Chem. B*, 2001, **105**, 8350–8355.
130 N. Ulagappan and H. Frei, *J. Phys. Chem. A*, 2000, **104**, 7834–7839.
131 W.-J. Yin, S. Chen, J.-H. Yang, X.-G. Gong, Y. Yan and S.-H. Wei, *Appl. Phys. Lett.*, 2010, **96**, 221901–221903.
132 I. Nakamura, N. Negishi, S. Kutsuna, T. Ihara, S. Sugihara and K. Takeuchi, *J. Mol. Catal. A: Chem.*, 2000, **161**, 205–212.
133 H. Irie, Y. Watanabe and K. Hashimoto, *Chem. Lett.*, 2003, **32**, 772–773.
134 H. Weng, X. Yang, J. Dong, H. Mizuseki, M. Kawasaki and Y. Kawazoe, *Phys. Rev. B: Condens. Matter Mater. Phys.*, 2004, **69**, 125219.
135 Y. Gai, J. Li, S.-S. Li, J.-B. Xia and S.-H. Wei, *Phys. Rev. Lett.*, 2009, **102**, 036402.
136 R. Long and N. J. English, *Appl. Phys. Lett.*, 2009, **94**, 132102–132103.
137 E. Fazio, P. Calandra, V. T. Liveri, N. Santo and S. Trusso, *Colloids Surf., A*, 2011, **392**, 171–177.
138 H. W. N. Slamet, E. Purnama, K. Riyani and J. Gunlazuardi, *World Appl. Sci. J.*, 2009, **6**, 112–122.
139 K. Sayama and H. Arakawa, *J. Phys. Chem.*, 1993, **97**, 531–533.
140 M. Antoniadou, D. I. Kondarides and P. Lianos, *Catal. Lett.*, 2009, **129**, 344–349.
141 V. M. Daskalaki and D. I. Kondarides, *Catal. Today*, 2009, **144**, 75–80.
142 C. Ampelli, G. Centi, R. Passalacqua and S. Perathoner, *Energy Environ. Sci.*, 2010, **3**, 292–301.
143 M. Qamar, *Int. J. Nanosci.*, 2010, **9**, 579–583.
144 H. Shi and Z. Zou, *J. Phys. Chem. Solids*, 2012, **73**, 788–792.
145 P. Li, S. Ouyang, G. Xi, T. Kako and J. Ye, *J. Phys. Chem. C*, 2012, **116**, 7621–7628.
146 N. Zhang, S. Ouyang, P. Li, Y. Zhang, G. Xi, T. Kako and J. Ye, *Chem. Commun.*, 2011, **47**, 2041–2043.
147 O. Ishitani, C. Inoue, Y. Suzuki and T. Ibusuki, *J. Photochem. Photobiol., A*, 1993, **72**, 269–271.
148 F. Solymosi, I. Tombácz and J. Koszta, *J. Catal.*, 1985, **95**, 578–586.
149 I. Tseng, J. Wu and H.-Y. Chou, *J. Catal.*, 2004, **221**, 432–440.
150 I. Tseng, W.-C. Chang and J. Wu, *Appl. Catal., B*, 2002, **37**, 37–48.
151 K. Adachi, K. Ohta and T. Mizuno, *Sol. Energy*, 1994, **53**, 187–190.
152 K. Kočí, K. Matějů, L. Obalová, S. Krejčíková, Z. Lacný, D. Plachá, L. Čapek, A. Hospodková and O. Šolcová, *Appl. Catal., B*, 2010, **96**, 239–244.
153 S. Krejčíková, L. Matějová, K. Kočí, L. Obalová, Z. Matěj, L. Čapek and O. Šolcová, *Appl. Catal., B*, 2012, **111**, 119–125.
154 K. Iizuka, T. Wato, Y. Miseki, K. Saito and A. Kudo, *J. Am. Chem. Soc.*, 2011, **133**, 20863–20868.
155 P. Ji, M. Takeuchi, T.-M. Cuong, J. Zhang, M. Matsuoka and M. Anpo, *Res. Chem. Intermed.*, 2010, **36**, 327–347.
156 M. Alvaro, C. Aprile, B. Ferrer, F. Sastre and H. García, *Dalton Trans.*, 2009, 7437–7444.
157 C. Aprile, M. Á. Herranz, E. Carbonell, H. Garcia and N. Martín, *Dalton Trans.*, 2009, 134–139.
158 G. Guan, T. Kida and A. Yoshida, *Appl. Catal., B*, 2003, **41**, 387–396.
159 A. Nishimura, G. Mitsui, M. Hirota and E. Hu, *Int. J. Chem. Eng.*, 2010, **2010**, 1–9.
160 R. Dholam, N. Patel, M. Adami and A. Miotello, *Int. J. Hydrogen Energy*, 2009, **34**, 5337–5346.
161 L. Pan, J.-J. Zou, X. Zhang and L. Wang, *Ind. Eng. Chem. Res.*, 2010, **49**, 8526–8531.
162 C.-C. Yang, J. Vernimmen, V. Meynen, P. Cool and G. Mul, *J. Catal.*, 2011, **284**, 1–8.
163 J.-S. Hwang, J.-S. Chang, S.-E. Park, K. Ikeue and M. Anpo, *Top. Catal.*, 2005, **35**, 311–319.
164 S. S. Srinivasan, J. Wade, E. K. Stefanakos and Y. Goswami, *J. Alloys Compd.*, 2006, **424**, 322–326.
165 J. Wu, *Appl. Catal., A*, 2008, **335**, 112–120.
166 J. Wu, *Sol. Energy Mater. Sol. Cells*, 2008, **92**, 864–872.
167 Q. Zhai, S. Xie, W. Fan, Q. Zhang, Y. Wang, W. Deng and Y. Wang, *Angew. Chem., Int. Ed.*, 2013, **125**, 5888–5891.
168 O. K. Varghese, M. Paulose, T. J. LaTempa and C. A. Grimes, *Nano Lett.*, 2009, **9**, 731–737.
169 B. D. Mankidy, B. Joseph and V. K. Gupta, *Nanotechnology*, 2013, **24**, 405402.
170 C. Wang, Z. Xie, K. E. deKrafft and W. Lin, *J. Am. Chem. Soc.*, 2011, **133**, 13445–13454.
171 M. Anpo, H. Yamashita, K. Ikeue, Y. Fujii, S. G. Zhang, Y. Ichihashi, D. R. Park, Y. Suzuki, K. Koyano and T. Tatsumi, *Catal. Today*, 1998, **44**, 327–332.
172 J. Hemminger, R. Carr and G. Somorjai, *Chem. Phys. Lett.*, 1978, **57**, 100–104.
173 M. Hamadanian, A. Reisi-Vanani and A. Majedi, *Mater. Chem. Phys.*, 2009, **116**, 376–382.
174 C. Wen, Y.-J. Zhu, T. Kanbara, H.-Z. Zhu and C.-F. Xiao, *Desalination*, 2009, **249**, 621–625.
175 L. Zhou, J. Deng, Y. Zhao, W. Liu, L. An and F. Chen, *Mater. Chem. Phys.*, 2009, **117**, 522–527.
176 S. In, A. Orlov, R. Berg, F. García, S. Pedrosa-Jimenez, M. S. Tikhov, D. S. Wright and R. M. Lambert, *J. Am. Chem. Soc.*, 2007, **129**, 13790–13791.

177 S. U. Khan, M. Al-Shahry and W. B. Ingler, *Science*, 2002, **297**, 2243–2245.
178 J. C. Yu, J. Yu, W. Ho, Z. Jiang and L. Zhang, *Chem. Mater.*, 2002, **14**, 3808–3816.
179 G. Wu, J. Wen, J. Wang, D. F. Thomas and A. Chen, *Mater. Lett.*, 2010, **64**, 1728–1731.
180 M. Pelaez, A. A. de la Cruz, E. Stathatos, P. Falaras and D. D. Dionysiou, *Catal. Today*, 2009, **144**, 19–25.
181 M. Tahir and N. S. Amin, *Energy Convers. Manage.*, 2013, **76**, 194–214.
182 T. M. Suzuki, H. Tanaka, T. Morikawa, M. Iwaki, S. Sato, S. Saeki, M. Inoue, T. Kajino and T. Motohiro, *Chem. Commun.*, 2011, **47**, 8673–8675.
183 S. Sato, T. Morikawa, S. Saeki, T. Kajino and T. Motohiro, *Angew. Chem., Int. Ed.*, 2010, **49**, 5101–5105.
184 C.-W. Tsai, H. M. Chen, R.-S. Liu, K. Asakura and T.-S. Chan, *J. Phys. Chem. C*, 2011, **115**, 10180–10186.
185 L. M. Xue, F. H. Zhang, H. J. Fan and X. F. Bai, *Adv. Mater. Res.*, 2011, **183**, 1842–1846.
186 H. Irie, S. Washizuka and K. Hashimoto, *Thin Solid Films*, 2006, **510**, 21–25.
187 T. Ohno, M. Akiyoshi, T. Umebayashi, K. Asai, T. Mitsui and M. Matsumura, *Appl. Catal., A*, 2004, **265**, 115–121.
188 D. Li, H. Haneda, S. Hishita, N. Ohashi and N. K. Labhsetwar, *J. Fluorine Chem.*, 2005, **126**, 69–77.
189 Z. He, L. Xie, S. Song, C. Wang, J. Tu, F. Hong, Q. Liu, J. Chen and X. Xu, *J. Mol. Catal. A: Chem.*, 2010, **319**, 78–84.
190 Q. Zhang, Y. Li, E. A. Ackerman, M. Gajdardziska-Josifovska and H. Li, *Appl. Catal., A*, 2011, **400**, 195–202.
191 V. Heleg-Shabtai, E. Zahavy and I. Willner, *Energy Convers. Manage.*, 1995, **36**, 609–612.
192 Z. Li, Y. Zhou, J. Zhang, W. Tu, Q. Liu, T. Yu and Z. Zou, *Cryst. Growth Des.*, 2012, **12**, 1476–1481.
193 J. Pan, X. Wu, L. Wang, G. Liu, G. Q. M. Lu and H.-M. Cheng, *Chem. Commun.*, 2011, **47**, 8361–8363.
194 J. C. Wu, *Catal. Surv. Asia*, 2009, **13**, 30–40.
195 J. Wu and C.-H. Chiou, *Catal. Commun.*, 2008, **9**, 2073–2076.
196 O. Ozcan, F. Yukruk, E. Akkaya and D. Uner, *Top. Catal.*, 2007, **44**, 523–528.
197 J.-M. Lehn and R. Ziessel, *Proc. Natl. Acad. Sci. U. S. A.*, 1982, **79**, 701–704.
198 T. Hirose, Y. Maeno and Y. Himeda, *J. Mol. Catal. A: Chem.*, 2003, **193**, 27–32.
199 C. Wang, R. L. Thompson, P. Ohodnicki, J. Baltrus and C. Matranga, *J. Mater. Chem.*, 2011, **21**, 13452–13457.
200 C. Wang, R. L. Thompson, J. Baltrus and C. Matranga, *J. Phys. Chem. Lett.*, 2009, **1**, 48–53.
201 W. A. Tisdale, K. J. Williams, B. A. Timp, D. J. Norris, E. S. Aydil and X.-Y. Zhu, *Science*, 2010, **328**, 1543–1547.
202 R. Seoudi, G. El-Bahy and Z. El Sayed, *Opt. Mater.*, 2006, **29**, 304–312.
203 Z. Zhao, J. Fan, M. Xie and Z. Wang, *J. Cleaner Prod.*, 2009, **17**, 1025–1029.
204 Z. Zhao, J. Fan, S. Liu and Z. Wang, *Chem. Eng. J.*, 2009, **151**, 134–140.
205 Z.-H. Zhao, J.-M. Fan and Z.-Z. Wang, *J. Cleaner Prod.*, 2007, **15**, 1894–1897.
206 Q. Wang, W. Wu, J. Chen, G. Chu, K. Ma and H. Zou, *Colloid Surf., A*, 2012, **409**, 118–125.
207 J. Ettedgui, Y. Diskin-Posner, L. Weiner and R. Neumann, *J. Am. Chem. Soc.*, 2010, **133**, 188–190.
208 T. W. Woolerton, S. Sheard, E. Reisner, E. Pierce, S. W. Ragsdale and F. A. Armstrong, *J. Am. Chem. Soc.*, 2010, **132**, 2132–2133.
209 T. W. Woolerton, S. Sheard, E. Pierce, S. W. Ragsdale and F. A. Armstrong, *Energy Environ. Sci.*, 2011, **4**, 2393–2399.
210 H. Arakawa, M. Aresta, J. N. Armor, M. A. Barteau, E. J. Beckman, A. T. Bell, J. E. Bercaw, C. Creutz, E. Dinjus and D. A. Dixon, *Chem. Rev.*, 2001, **101**, 953–996.
211 W. Hou, W. H. Hung, P. Pavaskar, A. Goeppert, M. Aykol and S. B. Cronin, *ACS Catal.*, 2011, **1**, 929–936.
212 W.-N. Wang, J. Park and P. Biswas, *Catal. Sci. Technol.*, 2011, **1**, 593–600.
213 D. Luo, Y. Bi, W. Kan, N. Zhang and S. Hong, *J. Mol. Struct.*, 2011, **994**, 325–331.
214 H.-C. Yang, H.-Y. Lin, Y.-S. Chien, J. C.-S. Wu and H.-H. Wu, *Catal. Lett.*, 2009, **131**, 381–387.
215 J. C. Wu, T.-H. Wu, T. Chu, H. Huang and D. Tsai, *Top. Catal.*, 2008, **47**, 131–136.
216 I. Tseng and J. C.-S. Wu, *Catal. Today*, 2004, **97**, 113–119.
217 K. R. Thampi, J. Kiwi and M. Graetzel, *Nature*, 1987, **327**, 506–508.
218 J. Jensen, M. Mikkelsen and F. C. Krebs, *Sol. Energy Mater. Sol. Cells*, 2011, **95**, 2949–2958.
219 P. Gijsman, G. Meijers and G. Vitarelli, *Polym. Degrad. Stab.*, 1999, **65**, 433–441.
220 C. Jin, P. Christensen, T. Egerton, E. Lawson and J. White, *Polym. Degrad. Stab.*, 2006, **91**, 1086–1096.
221 R. E. Kesting, *Synthetic polymeric membranes: a structural perspective*, Wiley, New York, 2nd edn, 1985.
222 S. Fernando, P. Christensen, T. Egerton, R. Eveson, S. Martins-Franchetti, D. Voisin and J. White, *Mater. Sci. Technol.*, 2009, **25**, 549–555.
223 W. Kim, T. Seok and W. Choi, *Energy Environ. Sci.*, 2012, **5**, 6066–6070.
224 T. Arai, S. Tajima, S. Sato, K. Uemura, T. Morikawa and T. Kajino, *Chem. Commun.*, 2011, **47**, 12664–12666.